A Numerical Study on the Influences of Sumatra Topography and Synoptic Features on Tropical Cyclone Formation over the Indian Ocean

Chung-Chieh Wang[1], Shin-Kai Ma[1], and Richard H. Johnson[2]

1 Department of Earth Sciences, National Taiwan Normal University, Taipei, Taiwan

2 Department of Atmospheric Sciences, Colorado State University, Fort Collins, CO, USA

Submitted to

Monthly Weather Review

14 July 2019

* *Corresponding Author address:* Prof. Chung-Chieh Wang, Department of Earth Sciences, National Taiwan Normal University. No. 88, Sec. 4, Ting-Chou Rd., Taipei, 11677 Taiwan. E-mail: cwang@ntnu.edu.tw

Abstract

Sitting across the Equator with a northwest-southeast orientation, the island of Sumatra can exert significant influences on low-level flow. Under northeasterly flow, in particular, lee vortex can form and some of them may subsequently develop into tropical cyclones (TCs) in the Indian Ocean (OI). Building upon the recent work of Fine et al., this study investigates the roles of the Sumatra topography and other common features on the formation of selected cases for analysis and numerical experiments.

Four cases in northern IO were selected for analysis and two of them (Nisha and Ward) for simulation at a grid size of 4 km. Sensitivity tests without the Sumatra topography were also performed. Our results indicate that during the lee stage, the pre-TC vortices are indeed mostly stronger with a clearer circulation due to the presence of Sumatra. However, the island's terrain is helpful but not a deciding factor on TC formation, as after shedding, the vortices in the no-terrain tests also reach TC status, just at a later time. Some common ingredients contributing to a favorable environment for TC genesis are identified, and include: northeasterly winds near northern Sumatra, westerly wind bursts along the equator, and migratory disturbances (TC remnants or Borneo vortices) to provide additional vorticity/moisture from the South China Sea. These factors also appear in most of the 22 TC cases in northern IO during October-December in 2008 and 2009. For the sole case (Cleo) examined in southern IO, the deflection of equatorial westerlies into northwesterlies by Sumatra (on the windward side) is also found helpful to TC formation.

1. Introduction

The formation of tropical cyclone (TC) is regarded as a complex process that involves continuous and nonlinear interaction among mechanisms across a wide range of scales, rather than controlled by a single mechanism. Since Ooyama (1982), tropical cyclogenesis is considered the transition from the probabilistic to deterministic stage in the lifecycle of a TC. In the probabilistic stage with weak relative vorticity ζ (and absolute vorticity η), tropical cloud clusters typically have large Rossby radius of deformation (λ_R) and low heating efficiency from latent heat release, and most of them have short lifespan and do not intensify into TCs.

Past studies have established the synoptic conditions conducive to TC formation (e.g., Gray 1968): Deep ocean mixing layer with sea-surface temperature (SST) at least 26.5°C, unstable atmospheric environment, high moisture content in low and middle levels, weak vertical wind shear, a latitude outside 5° (non-zero Coriolis force), and higher low-level vorticity. However, even when all the above conditions are met, in the probabilistic stage, it only means a higher likelihood for TC genesis. The cloud cluster (and initial vortex) still needs external forcing mechanism(s) to increase its vorticity, reduce the λ_R, and subsequently raise the heating efficiency of cumulus convection. Only after that, the disturbance can survive the probabilistic stage and enter the deterministic stage with positive feedback in development through the mechanism of Conditional Instability of the Second Kind (CISK; Ooyama 1982) or Wind-Induced Surface Heat Exchange (WISHE; Emanuel 1986; Rotunno and Emanuel 1987).

For individual disturbances, some external forcing mechanism, or mechanisms, is an essential element for TC formation, besides favorable environmental conditions. In the western North Pacific (WNP), for example, Ritchie and Holland (1999) identified five types in large-scale circulation that can force or are linked to TC formation: Monsoon shear line,

monsoon gyre, easterly wave, monsoon confluence region, and Rossby energy dispersion. The observational study of Lee (1986) also points out the importance of low-level momentum forcing in TC-genesis cases in WNP. Such momentum forcing over a large area may come from cross-equatorial flow, Trade Wind surge, or burst of Indian monsoon. Through inward transfer of eddy vorticity flux, the forcing can increase the low-level ζ of the TC vortex without a strengthening in its transverse circulation, and act to help the TC to enter the deterministic stage (Lee 1986).

Mid-latitude cold-air outbreaks in the opposing hemisphere are usually the source of the cross-equatorial flow (Love 1985a,b), while those in the same hemisphere is one possible reason for the Trade Wind surge. In northern Indian Ocean (NIO) where TCs occur more often during pre-monsoon and post-monsoon seasons (e.g., Subbaramayya and Rao 1984; Kikuchi and Wang 2010), similar low-level momentum forcings from equatorward or poleward wind bursts also often promote TC formation there (Lee et al. 1989), and the initially asymmetric shearing vorticity gradually turns into symmetric curvature vorticity as the vortex grows stronger. In addition, when a TC forms and intensifies in the Indian Ocean (IO), its outer circulation can enhance the shearing vorticity in the other hemisphere and this may lead to TC formation there, and thus a TC pair across the equator (Lee et al. 1989).

The cold surge helps TC formation not only in WNP and NIO, but also in the South China Sea (SCS; Chang et al. 2004; Lin and Lee 2011). In the winter, when the northeasterly wind surge reaches the SCS, it may provide positive vorticity and lead to the formation of the Borneo vortex (BV). Some semi-stationary and others moving westward, the Borneo vortices may continue to develop and eventually become a TC if the environment is favorable (Lin and Lee 2011). One such example is Typhoon Vamei (2001) that formed near Singapore and very close to the equator (Chang et al. 2003). Through composite analysis, Takahashi et al. (2011) also found that regions of positive vorticity often exist in the SCS and NIO due to strong

northeasterly flow during the winter months (October-March), and thus the northeasterly monsoon flow can be influential to TC formation in the SCS and NIO.

In additional to the large-scale momentum forcing mentioned above, certain topographic features in the tropics can act to produce localized vorticity, and therefore play a role in TC formation. One such feature is the Central America (Sierra Madre in particular), which is verified to affect the formation of hurricanes downstream from the topography in eastern North Pacific (Mozer and Zehnder 1996; Farfán and Zehnder 1997; Zehnder et al. 1999). Results from numerical experiments indicate that lee vortices (Smolarkiewicz and Rotunno 1989; Rotunno and Smolarkiewicz 1991; Epifanio 2003), with a depth of about 3 km, often form in a low-Froude number (*Fr*) regime under easterly prevailing wind. The definition of *Fr*, which gives the overall response of the flow when encountering an obstacle, is $Fr = U/Nh$, where U is the wind speed perpendicular to the topography, N is buoyancy oscillation frequency, and h is the terrain height. For Central America, both the strong jet through the mountain gap and the flow around the topography due to its blocking effect can produce vorticity to form lee vortices under such conditions. With moisture advection from the Intertropical Convergence Zone (ITCZ), the environment downstream from Central America may become even more favorable to TC development (Zehnder et al. 1999). The above case studies indicate the topography can produce the initial vortex, which can develop into a TC given a suitable environment.

Compared to the Central America, the topography of Sumatra at the western end of maritime continent is much less studied. Kuettner (1967, 1989) suggests that the unique configuration of Sumatra, which straddles the equator and found nowhere else in the world, may be an important source for TC pairs in the IO. With a northwest-southeast orientation, the topography of Sumatra extends more than 1600 km (from about 6°N to 6°S) and peaks at about 3.8 km (cf. Fig. 1a). When the winter northeasterly flow reaches Sumatra, lee vortices

may form at both ends. While counter-rotating but both cyclonic, they may serve as initial vortices and, after shedding, intensify into TCs under favorable environment (Fig. 1a).

Recently, Fine et al. (2016) examined TCs in IO using datasets from European Center for Medium-Range Weather Forecasts (ECMWF) Year of Tropical Convection (YOTC, 2008-2010; Waliser et al. 2012) and Dynamics of the Madden-Julian Oscillation (DYNAMO, 2011-2012; Johnson and Ciesielski 2013). They found that 31.3% of all TCs in the 2.5-yr study period in NIO can be traced back to the Sumatra area, while the corresponding number is 22.9% for those in southern IO (SIO). These high percentages imply that the topography of Sumatra could play a significant role in providing initial vortices of TCs in IO. For northern (southern) Sumatra, the terrain-induced cyclonic vortices are more common during boreal winter (summer) with low-level easterly flow, while TC genesis from them in NIO appear to occur in October-December (Fine et al. 2016), presumably link to other environmental factors.

Building upon the observational study of Fine et al. (2016), the present study selects a few lee vortex cases that developed into named TCs during the YOTC period for analysis and numerical simulation. Sensitivity experiments in which the Sumatra topography is removed are also performed, with a goal to clarify the importance of the topography relative to other potentially helpful factors for TC formation in these cases. Present in all cases selected herein, these other factors include certain synoptic ingredients surrounding the lee area and vorticity and moisture advection associated with incipient disturbances, such as a BV, from the SCS upstream. So far, numerical study on the process in which a wake vortex of Sumatra developing into a TC has not yet been performed, nor on the relative importance of Sumatra topography and other synoptic features in the environment.

2. Data and design of numerical experiments

a. Data and analysis methods

In this study, all the TCs in NIO during October-December within the YOTC period (May 2008-April 2010, Waliser et al. 2012; Moncrieff et al. 2012) were briefly analyzed (sections 3 and 6), and their basic track and intensity information was taken from the Joint Typhoon Warning Center (JTWC) best-track data. The gridded ECMWF-YOTC global analyses (e.g., Moncrieff et al. 2012), available on a $0.25° \times 0.25°$ (latitude-longitude) grid at 20 levels (1000 to 10 hPa) every 6 h, were used for this examination on the synoptic environment and evolution of these storms.

From the 13 cases included in Fine et al. (2016), five TCs were selected for a more detailed analysis on the processes of lee vortex formation and the subsequent TC genesis using the ECMWF-YOTC data in section 3. The stronger three TCs, including Nisha (2008) and Ward (2009) in NIO and Cleo (2009) in SIO, were further chosen for numerical simulation and sensitivity tests, for which the ECMWF-YOTC data also served as initial and boundary conditions (IC/BCs). While the model used and the experiments will be described shortly, satellite brightness temperature (T_B) imageries provided by the Naval Research Laboratory (NRL) and microwave products from the Space Science and Engineering Center (SSEC, at University of Wisconsin) were also used to help verify model simulations.

In this study, the intensity of tropical storm (TS) of 34 kts was adopted to identify TC formation in both the observation and model in a consistent way, as the storms are given a name and typically enter the deterministic stage near this time (Ooyama 1982). To analyze their vertical structure and evolution, the center of the vortices at (or near) 850 hPa was identified and used to compute the mean relative vorticity within a radius of 550 km, including the earlier, lee stage of the vortices. To further diagnose the differences between the control experiment and sensitivity test (without the Sumatra terrain) of each TC case, the vorticity equation was employed, and a lag correlation analysis between the vorticity of the

lee vortex and the upstream *Fr* was also carried out to elucidate the topographic effects of the Sumatra Island. Further details of these analyses will be described in sections 4 and 5.

b. Numerical model and experiments

The Cloud-Resolving Storm Simulator (CReSS) version 3.4.2 (Tsuboki and Sakakibara 2002, 2007) is used in this study for all experiments. It is a single-domain, non-hydrostatic and compressible cloud-resolving model with a terrain-following vertical coordinate. In CReSS, clouds are explicitly treated using a bulk cold-rain microphysics scheme with a total of six species (vapor, cloud water, cloud ice, rain, snow, and graupel) without the use of any cumulus parameterization, while subgrid-scale processes such as turbulent mixing in the boundary layer and surface radiation and momentum/energy fluxes are parameterized (Table 1). The CReSS model has been employed in many earlier studies on TCs (Wang 2015; Wang et al. 2012; 2013; 2015; 2016; Chen et al. 2017; Kuo et al. 2019), and the readers are referred to the references therein and Tsuboki and Sakakibara (2002, 2007) for further details.

Two control (CTL) experiments were performed using a large domain of 5600 km × 4464 km (roughly 20°S-20°N, 70°-120°E, Fig. 1b) at a convective-permitting grid size of 4 km, one for Nisha (2008) and the other for Ward (2009) and Cleo (2009) together, since they were twin cyclones across the equator during the same period. Using the YOTC analyses as IC/BCs, these runs started from 6 h before the arrival of low-level northeasterly flow to Sumatra, and lasted for 15 days for Nisha (2008) and 16 days for Ward and Cleo (2009), respectively (cf. Table 1). For the no-terrain (NT) tests, all model setups are identical to the CTL, except that the topography of Sumatra (and small islands nearby) are removed (but the land mass remains, cf. Fig. 1a). Here, it should be noted that the SIO case of Cleo was not a lee vortex, since the northeasterly flow did not extend south of the equator. In fact, none of the SIO TCs examined by Fine et al. (2016) developed from a lee vortex, but as the only SIO case, it is still worthwhile to include Cleo in the present study.

c. Vorticity budget analysis for lee vortices

Except for the methods mentioned above in section 2a, the vorticity budget analysis was also performed for the vortices during the lee stage in both CTL and NT experiments for each of the selected cases to further shed lights on their development. The vorticity (tendency) equation in *z* coordinate can be written as

$$\frac{\partial \zeta}{\partial t} = -\vec{\mathbf{V}} \cdot \nabla \eta - w\frac{\partial \zeta}{\partial z} - \eta(\nabla \cdot \vec{\mathbf{V}}) + \left(\frac{\partial u}{\partial z}\frac{\partial w}{\partial y} - \frac{\partial v}{\partial z}\frac{\partial w}{\partial x}\right) + \frac{1}{\rho^2}\left(\frac{\partial \rho}{\partial x}\frac{\partial p}{\partial y} - \frac{\partial \rho}{\partial y}\frac{\partial p}{\partial x}\right) + \left(\frac{\partial F_y}{\partial x} - \frac{\partial F_x}{\partial y}\right) \quad (1)$$

where the forcing terms on the RHS, following their order, are horizontal advection of η (= ζ + f), vertical transfer of ζ, convergence (or vertical stretching) effect, tilting effect, solenoidal effect, and the frictional effect that also accounts for the residual from computational errors. All the variables and parameters in Eq. (1) have their usual meaning in meteorology. Using Eq. (1), the model results of lee vortices in CTL and NT experiments are compared (sections 4 and 5).

3. Case analysis

Five TCs were selected for analysis in this section, and they are TC 03A (2008), TS Nisha (2008), TC 07B (2008), TS Ward (2009), and TC Cleo (2009), respectively, in chronic order. The first four were in NIO and developed into TCs from lee vortices of northern Sumatra, while Cleo was in SIO and formed a TC pair with Ward as mentioned. The full tracks of these five cases, constructed using both YOTC analysis (vortex center at 850 hPa during pre-TS stage) and JTWC best-track data (TS and beyond), are shown in Fig. 1b.

Following the methodology described in section 2, time-height section of relative vorticity ζ for the four cases in NIO were constructed (Fig. 2). This allowed us to identify the level of maximum (areal-mean) ζ during the leeside stage of the vortices, and these levels were used to show (in Fig. 3) the evolution in wind and vorticity before, at, and after the

formation of leeside vortex (t_0), which is taken to be the time when a closed circulation formed in the ECMWF-YOTC analysis. During the 4-day period, easterly flow appeared near northern Sumatra and to its north in all four cases and mostly strengthened (Fig. 3), while westerly winds intensified at lower latitudes near the Equator prior to t_0, except for 03A in which the same occurred shortly after t_0 (Fig. 3a). Appearing also in the composite fields of Fine et al. (2016, their Figs. 2a and 6), these two branches of airflow provided cyclonic vorticity and a background environment favorable for lee vortex formation and its subsequent development.

In addition to the opposing flow in the leeside region, clear incipient positive vorticity also existed in Fig. 3 near 110°E at 0°-5°N in the SCS two days before lee vortex formation in all three latter cases, while the one in 03A was weaker and less evident (Fig. 3a). These vorticity centers were either from the remnant of a tropical system or associated with a BV, and moved westward to reach the leeside of northern Sumatra at t_0, when the lee vortex subsequently formed. Afterward, the lee vortex in all four cases gradually shed and moved downstream, away from Sumatra (Fig. 3). In longitude-time (Hovmoller) plots (Fig. 4), the incipient disturbances can be readily identified to be from the remnants of a tropical depression for 03A, the remnants of TS Maysak for Nisha, and a BV for both 07B and Ward, respectively, and they also carried a higher moisture content (in total precipitable water) into the lee area or its vicinity (Fig. 4, right column). For the latter two cases, the vorticity associated with the incipient BV was stronger with a wider circulation (Figs. 3c,d) and maximized further aloft near 500-600 hPa around t_0 (Figs. 2c,d). Afterwards, as the vortex shed, it developed downward toward the surface and the low-level ζ strengthened (Fig. 2). Apparently, these migratory synoptic disturbances provided incipient vorticity and moisture and were also helpful to the development of lee vortex, and subsequently the TC at a later time (e.g., Gray 1968).

Figure 5 presents the 925-hPa flow fields and precipitable water amount in a larger domain at t_0 for the four NIO cases. Except for 03A, which had a weaker flow, strong northeasterly or northerly winds from cold air surges from mid-latitudes were present over SCS and Malay Peninsula in all other three cases (Figs. 5b-d). The relatively dry cold air became easterly as it traveled south, and could reach the northern tip of Sumatra at this time. Meanwhile, along the equator, there existed a westerly wind burst (WWB) at low-levels in these three cases. Interestingly, a pair of synoptic-scale vortices were also present across the equator in the IO (red dashed circles in Fig. 5) in each case, and their circulation (with enhanced horizontal pressure gradient) evidently helped the equatorial westerlies to intensify, in a way previously pointed out by Lee et al. (1989). In addition to some known factors such as the Madden-Julian Oscillation or equatorial waves (Wang and Moon 2017), such vortex pairs in the IO clearly can also be the cause of WWB along the equator and thus affect our cases.

In all four cases, low-level southeasterly flow prevailed over a vast area south and southwest of Sumatra (Fig. 5). Coupled with the westerly flow (or a weaker flow) along the equator, this could also provide cyclonic vorticity (in the Southern Hemisphere) for the region west of southern Sumatra, as shown in Figs. 5a,b,d (green dashed circles), also consistent with Lee et al. (1989) and Fine et al. (2016, their Fig. 7). The vortex west of southern Sumatra in Fig. 5d later developed into Cleo, which formed a vortex pair with Ward. As mentioned, the remnants of a TS or BV were associated with higher moisture content and in the SCS (white dashed circles in Fig. 5) at this time (for Nisha, 07B, and Ward), and would soon move into the leeside of northern Sumatra.

Thus, some common synoptic-scale features or ingredients can be identified from Figs. 3-5 for the four TC cases in NIO during their leeside stage, and they include low-level northeasterly wind surges in the SCS, WWB along the equator to the west of Sumatra, and an

incipient disturbance that brought stronger relative vorticity and higher moisture content into the lee area through horizontal advection. Among these features, the equatorial westerly winds were most likely also enhanced by the vortex pair (across the equator) when they developed. Below, the two stronger cases, i.e., TS Nisha (2008) and TC Ward (2009), are further selected for numerical simulation, for an investigation mainly to assess the relative importance of the topography of Sumatra, in particular to the subsequent TC formation. To achieve this goal, both CTL and NT experiments were performed for each case, and their results are compared in the following section.

4. Results of Nisha and Ward in northern Indian Ocean

a. Tropical Storm Nisha (2008)

For each case, the CTL experiment needs to be validated against the observations to ensure that the event is reproduced reasonably well. First, the modeled track and intensity for Nisha (2008) are shown in Fig. 6. Overall, the simulated track is fairly close to the track in the YOTC data, and the vortex first forms at the leeside of northern Sumatra and then moves westward and northwestward toward Sri Lanka and southern India, despite some discernible differences (Fig. 6a). In particular, the landfall points in Sri Lanka and southeastern India in CTL are quite close to the observation, an encouraging result for a model run 15 days in length. Similarly, reasonable results are obtained by the model for intensity of Nisha (Fig. 6b). In CTL, the timing to reach TS intensity (34 kts) is only about 1.5 days earlier than the JTWC data, while the modeled peak intensity (54 kts) on 26 November is also very close to the best track (50 kts). A deficit of about 10 hPa in the TC's minimum mean sea-level pressure (MSLP) appears after Nisha reached TS status, when the JTWC best track suggested 985 hPa (Fig. 6c). Overall, the simulation in track and intensity is quite reasonable.

In Fig. 7, the model outputs of column-maximum mixing ratio of precipitation (rain,

snow, plus graupel) are compared to the SSMI brightness temperature for rainband structure of TS Nisha. Even though the two quantities are not identical, the figure provides verification that the model well-reproduced the storm structure of Nisha before and during its TS stage (25-27 November) near Sri Lanka, including the general location of major rainbands and their asymmetrical structure more in the northern quadrants of the storm (Fig. 7).

The time-height section (0-12.3 km) of ζ for the vortex in CTL, also averaged inside 550 km from the center, is presented in Fig. 8a and can be compared with Fig. 2b, which is from the YOTC data. Overall, the two plots are very similar in both the magnitude and vertical structure of the areal-mean ζ, but some differences still exist. In particular, the model vortex appears weaker than that in the ECMWF-YOTC analyses during its leeside stage, especially in the lower levels and on the first day (17 November). After the vortex starts to shed, the CTL result agrees closely with the ECMWF in areal-mean ζ (Figs. 2b and 8a), and Nisha in CTL reaches TS intensity at 0000 UTC 24 November, roughly 42 h before the time issued by JTWC (Fig. 6b) as mentioned earlier.

When the terrain of Sumatra is removed in the NT experiment, the simulated track remains close to that in CTL (Fig. 6a). At first glance, the time-height ζ inside 550 km for Nisha in the two runs also appear similar, including the lee stage (Figs. 8a,b). Their differences, many quite subtle, can be better depicted in Fig. 8c (CTL minus NT), where the areal-mean ζ at low levels in CTL is stronger than that in NT for much of the time since 17 November, especially over 21-26 November as the vortex strengthens to reach the TS status. In agreement with Fig. 8c, the near-surface flows (below 1 km) in CTL also produce a stronger vorticity belt and a clearer vortex circulation center on 21 November (figure not shown). This result is consistent with Epifanio and Durran (2001), who suggest that topography can form corner flow and provide stronger shear vorticity to the downstream area. With a weaker mean ζ, the maximum wind speed associated with Nisha in NT is weaker than

that in CTL over 21-27 November (Fig. 6b), often by 5-10 kts, and the storm reaches TS intensity on 25 November, more than one day (27 h) later than in CTL. Even though the storm in CTL is stronger through much of its lifespan (Figs. 6b,c), the one in NT does also reach the TS status when the topography of Sumatra is removed.

To gain insight into the development of the lee vortex in CTL and to contrast it with the one in NT, a vorticity budget analysis (cf. section 2c) is performed on the vortex at a height of 1547 m (near 850 hPa), averaged also inside a radius of 550 km from the center, for its lee stage as shown in Fig. 9. For the pre-Nisha lee vortex in CTL (1200 UTC 15 to 0000 UTC 18 November 2008, t = 24-84 h), it is seen that the mean ζ at 1547 m (dashed curve) generally increases with time during this 60-h period, roughly from 0.8 to 1.7 $\times$ 10^{-5} s^{-1} (Fig. 9a), and it is mainly contributed by two terms: convergence/stretching (green) and vertical transfer (brown). The convergence effect is counteracted (out of phase) by horizontal advection (blue) as the same low-level inflow also tends to bring in lower ζ values from larger radii, while the vertical transfer is largely cancelled by the tilting term (red) since the stronger upward motion at the vortex center also tilt the vorticity vector from the vertical (rotation on xy-plane) into horizontal direction (rotation on vertical plane). While all the above four terms can reach around 2 $\times$ 10^{-9} s^{-2} in their peak magnitude, the friction/residual term is significantly smaller and the solenoidal effect is negligible. As a result, the local tendency of ζ in Fig. 9a (computed using time differentiation) is a relatively small net difference among the larger RHS terms with opposite signs, but is mostly positive to cause the gradual increase in ζ. While the budget results exhibit similar characteristics in the NT run (Fig. 9b), the convergence and vertical transfer terms are often smaller than in CTL, particularly on 17 November when the mean ζ at 1547 m starts to show larger differences (cf. Fig. 8c). The increase in both the convergence and vertical transfer terms in CTL on 17 November indicate that the two effects work in phase. In short, the results here suggest that the Sumatra

topography indeed is helpful to produce a stronger pre-Nisha vortex at the leeside, and as a result, Nisha reaches the TS status 27 h earlier in CTL compared to its counterpart in NT.

As reviewed in section 1, the blocking effect of Sumatra on the northeasterly flow can be characterized by *Fr*, and a larger (smaller) value favors the flow-over (flow-around) regime. Here, *h* is set to 1895 m obtained for northern Sumatra, and the mean *U* and *N* values at 3°-7°N along 100°E below 2 km (dotted red line in Fig. 1a) are used. To elucidate the influence of *Fr* upstream on vorticity generation downstream to the lee, the correlation between *Fr* and lagged mean vorticity tendency at 1547 m (as in Fig. 9) are calculated using hourly model outputs and presented in Fig. 10a for the pre-Nisha vortex. In CTL, the correlation coefficient (green curve) is positive (and at least ~0.2) for all lag time within 24 h, but is higher over 18-24 h with a peak value of 0.46 at 23 h. This result indicates that an intensification in the low-level prevailing northeasterly flow would take some time to reach (or influence) the leeside, but generally helps to increase the vorticity there albeit other factors. Without the terrain in the NT run (but *h* is still set to 1895 m for consistency), on the other hand, the enhancement in northeasterly flow can contribute more rapidly and directly to the lee vortex (mainly by providing shear vorticity, cf. Fig. 3b), as the coefficient peaks at 0.69 at a lag time of only 3 h and remains >0.5 within 7 h. However, the coefficient drops rapidly to below 0.2 after 11 h and even to negative values later (Fig. 10a), so the influence does not last.

b. Tropical Storm Ward (2009)

For TS Ward (2009), the observed and modeled track and intensity are presented in Fig. 11. All four tracks (JTWC, ECMWF-YOTC, and the two model runs CTL and NT) are close to one another, with movement generally toward the west during 3-9 December and then toward the north during 9-12 December after shedding (Fig. 11a). As in JTWC, the storms eventually make landfall in central Sri Lanka from the east, though with some variations in

timing. The landfall time in ECMWF data is near 1800 UTC 12 December and about 40 h earlier than that in JTWC (1200 UTC 14 December), and a similar early landfall also occurs in the two CReSS experiments, near 1500 UTC in CTL and 1800 UTC in NT on 12 December. Again, at a range of nearly two weeks, such track errors (about 200 km) in Fig. 11a are in fact very small. Before landfall, all four data give almost identical timing, within a 6-h period, to reach the TS status on 11 December (Fig. 11b). The two simulations produce a maximum surface wind speed stronger than JTWC best-track, but the intensity quickly drops since 12 December (especially in CTL) due to the early landfall. Most likely for the same reason, the central MSLP in the model runs over 12-13 December are also not as low as that in JTWC (Fig. 11c), as they are closer to Sri Lanka than the observation. During 6-9 December when the pre-Ward vortex tracks westward, nevertheless, its intensity in CTL is mostly stronger in compared to NT (Fig. 11b).

For the period near landfall of Ward (11-12 December), the storm rainfall structure in CTL is compared with SSMI satellite observation in Fig. 12. Although the storm appears larger in the fields of column-maximum mixing ratio (Fig. 12, right column) compared to the satellite observed T_B (left column), the model successfully captures the general characteristics of rainfall structure, its asymmetry, and time evolution. These include an increasingly tighter and more symmetrical rain/cloud structure over 0200-1300 UTC 11 December as the storm intensified to reach TS (Fig. 12, upper half, cf. Fig. 11b), and soon afterwards a comma cloud shape that later deteriorated on 12 December as the storm moved closer to land (Fig. 12, bottom half).

The time-height cross section of areal-mean ζ inside the radius of 550 km in CTL for the vortex in the case of Ward, as shown in Fig. 13a, agree reasonably well with that constructed from ECMWF-YOTC analyses (cf. Fig. 2d), and both are weaker and do not extend upward as deep compared to the Nisha case (cf. Figs. 2b and 8a). Again, the time-height structure of ζ

in NT (Fig. 13b) is very close to CTL, and there is a tendency for downward development of ζ in the lee stage in both runs, from about 5 km toward the lower levels. While close, Fig. 13c still reveals that the vortex in CTL is stronger than that in NT during most of the lee stage that ends at 0000 UTC 4 December, except for a brief period around 0000 UTC 3 December. This difference in lee vortex strength is similar to the Nisha case (cf. Fig. 8c) but slightly more pronounced. However, such an advantage of CTL over NT does not maintain throughout the life span of Ward after shedding, and the storm in CTL reaches TS intensity only 4 h earlier than the one in NT (Fig. 11b).

The areal-mean vorticity budget (550 km from center) at 1547 m for the pre-Ward lee vortex (t = 24-96 h) in CTL (Fig. 14a) shows that the mean ζ is generally above 1.2×10^{-5} s^{-1} from 1800 UTC 30 November to 1200 UTC 2 December and mainly contributed by the convergence/stretching term (green), which is again largely cancelled by horizontal advection. In this case, the vertical transfer term (brown) can be either positive or negative in different time periods but remains out of phase from the tilting effect (red), which therefore also contributes toward ζ from time to time (when negative vertical transfer occurs). In NT, the ζ-budget calculation reveals similar results to CTL (Fig. 14b), but the contribution from convergence is generally smaller and the mean ζ grows to exceed 1.2×10^{-5} s^{-1} only toward the end, after about 1200 UTC 2 December. This is because a BV (visible in Figs. 3d, 4d, and 5d) is moving across the northern Sumatra (near 97°E) from upstream around this time, and without Sumatra's terrain, the lee vortex in NT moves eastward to merge with the BV (Fig. 11a), resulting in an increase in mean ζ and a stronger vortex in NT (versus CTL) near 3 December (Fig. 14). In contrast, with topography, the lee vortex in CTL remains stationary near 3 December, and a direct merger does not occur (Fig. 11a).

The results of lagged correlation between upstream Fr and areal-mean ζ at 1547 m at the leeside (east of 90°E and before 0600 UTC 2 December to exclude the influence from the BV)

indicate that for the pre-Ward lee vortex, the correlation coefficient (green) in CTL remains high within about 10 h and peaks at 0.54 with a 5-h lag time (Fig. 10b). On the other hand, the coefficient drops rapidly after only 3 h in NT, from a maximum of 0.47 at 1 h. Therefore, in both our simulated cases in NIO, the terrain exerts a longer, more persistent influence on the generation of leeside vorticity (through either subsidence warming or corner effect, or both) in CTL experiments, in comparison to NT runs where ζ is provided only through horizontal advection and/or shearing effect and for a shorter duration.

5. Results of Cleo in southern Indian Ocean

During the same period as Ward, another vortex also evolved into Cyclone Cleo in SIO as mentioned, so the same simulations (CTL and NT) are used to discuss its development as well here. Since the equatorial westerlies were present leading to the formation of this closed vortex to the west of southern Sumatra/western Java (Fig. 3d), the pre-Cleo vortex is not a lee vortex as pointed out by Fine et al. (2016). After formation, pre-Cleo first remained stationary for a few days, then moved toward the west-southwest quite steadily after 3 December (Fig. 15a). In CTL and NT, the corresponding vortices both form at the same location and time (at 0000 UTC 29 November) as the YOTC analysis, and also have a similar track. However, compared to observation, the vortex in CTL starts to move westward about 12-18 h too late, and even more so in NT (Fig. 15a). Later in the simulations after 1200 UTC 8 December, all tracks converge toward the JTWC with reduced track errors.

The JTWC best-track data indicate that Cleo reached TS intensity near 0000 UTC 7 December (Fig. 15b) but this occurs roughly 24 h later in CTL, and another 12 h later in NT, whose vortex moves out from its formation area the latest as mentioned. Both vortices, nonetheless, reach 34 kts at an earlier time but only briefly. After 1200 UTC 7 December, TC Cleo underwent a period of rapid intensification to reach a peak wind speed of over 110 kts

and a central MSLP of lower than 940 hPa (Figs. 15b,c). In the model, however, the storm is gradually approaching the domain boundary during this period (cf. Fig. 1b) and a similar intensification does not take place. Although not ideal, this is acceptable since our focus is on the formation and earlier stages of the vortex. For the period during 6-7 December, Cleo's rainfall structure in CTL is also compared with satellite observations, and the two are similar and in good agreement (Fig. 16).

The time-height cross sections of areal-mean ζ (inside 550 km) of the pre-Cleo vortex are again similar in CTL and NT runs (Fig. 17), where a downward development of ζ with time is evident before 5 December. In Fig. 17c, one can also see that the vortex in CTL is persistently stronger and extend deeper into the upper troposphere than that in NT during the stationary stage closer to Sumatra, but not so at low levels after 4-5 December. This latter difference, however, mainly exists only over outer regions at larger radii, as the peak 10-m wind at the inner core remains clearly stronger in CTL over 5-8 December (cf. Fig. 15b).

Prior to 0000 UTC 4 December (t = 48-120 h), the generation of mean vorticity is again mainly from convergence/stretching and vertical transfer terms (Fig. 18), which also tend to be greater in CTL than those in NT. In Fig. 19, the low-level mean winds below 2 km over the northeastern quadrant of the vortex (also within 550 km) in the two experiments are compared. Without the topography, the mean wind is between westerly and west-southwesterly in NT, but southwesterly in CTL. Thus, the Sumatra Island acts to block the equatorial westerly flow to provide a larger southward component and stronger curvature vorticity at low levels. This result is consistent with Fine et al. (2016), who speculated that the topography of Sumatra helps the vortex of pre-Cleo to gain strength. Thus, in the case of Cleo (2009) where its initial vortex is not at the leeside, the blocking effect of southern Sumatra on the equatorial westerlies, nevertheless, helps to provide stronger curvature vorticity and leads to a stronger, tighter and more compact vortex during it westward movement. Eventually, the storm in CTL

reaches the TS status 12 h before that in NT.

6. Discussion and conclusion

In the CTL experiments, the two lee vortices in NIO (Nisha and Ward) are generally stronger during the lee stage (Figs. 8 and 13) and subsequently reach the TS status earlier compared to their counterpart in NT runs (Fig. 6b), although the difference is small for Ward (Fig. 11b). Despite this, however, the storms in NT runs also reach the TS status (although slower) without the topography of Sumatra. This result indicates that the island of Sumatra is only a beneficial factor rather than a necessary condition for the formation of TCs, a conclusion that should not come as a surprise since the majority of named TCs in NIO do not originate from the leeside of Sumatra (e.g., Fine et al., 2016). It follows that some other factors common in both CTL and NT runs must play a more determinant role in the subsequent evolution and intensification of the vortex after vortex shedding. It is known that both a stronger initial vortex and favorable synoptic evolution surrounding it are important to TC genesis (section 1). In section 3, low-level northeasterly winds across or near northern Sumatra, equatorial WWB at low latitudes, and advection of vorticity and/or moisture from upstream into the lee area are seen to be the common ingredients in all four cases of 03A, Nisha, 07B, and Ward (Figs. 3-5). To find out how frequently these conditions/features occur for the TCs, here we use the ECMWF-YOTC data to check their occurrence in all 22 named storms in NIO during October-December in 2008 and 2009 following the same procedure as in section 3. The overall results are presented in Fig. 20.

In Fig. 20, the time series of equatorial westerly wind speed (averaged over 5°S-5°N, 80°-90°E) and northeasterly wind speed (averaged over 5°-10°N, 107°-115°E), both at 925 hPa, are shown together with the periods with named storms and those with vorticity (pink) and/or water vapor advection (orange) at 700 hPa. While the low-level northeasterly winds

generally strengthen from October to December and the equatorial westerly winds tend to be stronger in November, both of them are characterized by surges in pulses. During their early stage, the majority of vortices were associated with simultaneous surges in both northeasterly flow near northern Sumatra and equatorial westerly flow (Fig. 20). Among the seven cases that reached TS , the only exception is Phyan (2009), where the equatorial westerly was weak and only 2-3 m s^{-1} (Fig. 20b). During the formation stage, many disturbances were also accompanied by either vorticity or moisture advection, or both, especially in the Bay of Bangel (where many vortices originated from the leeside of Sumatra). Thus, not only in the four cases in section 3 (Figs. 2-5), the low-level environment that provided a background of cyclonic wind shear and the advection of vorticity/moisture from upstream into the area of initial vortex were also common features in nearly all cases in October-December of 2008 and 2009. Thus, these synoptic features are undoubtedly important factors for the development of initial vortices toward the TS/TC status in the NIO. Due to these favorable factors, in the cases of Nisha and Ward, a similar vortex can still develop to reach TS status in the NT runs even when Sumatra's topography is removed in the model. In East Pacific, an analogous situation exists, as many easterly wave disturbances there can be traced back to those from the North Atlantic crossing Central America (Rydbeck et al. 2017).

Based on the findings in this study, a modified conceptual model from that of Kuettner (1967, 1989; see Fig. 1a) is presented below in Fig. 21. In the NIO, the northeasterly wind (from upstream across the Malaysia Peninsula) near the northern tip of Sumatra combines with the equatorial westerly wind surge to provide a favorable background shear for the lee vortex to evolve. Frequently, the lee vortices are maintained and enhanced by incipient disturbances (a BV or TC/TS remnant) from the SCS, in the form of vorticity and/or moisture advection into the leeside. In these cases, the topography of Sumatra can provide additional help through flow deflection and lee cyclogenesis to further enhance the vorticity at leeside

during the lee stage, but it is not a necessary factor. For SIO, Cleo (2009) is the only storm studied herein. In this case, the northeasterly wind did not reach the southern latitudes, and southwestern Sumatra is in the windward side instead of leeside due to the equatorial westerly wind. However, Sumatra played a role to deflect the westerly wind southward and provide a larger vorticity together with the southeasterly trade wind further south. Thus, the hypothesis of Fine et al. (2016) is confirmed and the topography is also helpful for TC formation, and the synoptic conditions remain favorable for dual-vortex formation across the equator (as in the present case of Ward and Cleo). In contrast to the original model proposed by Kuettner (1967, 1989) in Fig. 1a, our conceptual model (Fig. 21) also includes the roles of equatorial westerly wind and upstream incipient disturbances from the SCS, with a different formation scenario for the vortex in SIO (not at leeside).

7. Summary and conclusion

Building upon the observational study of Fine et al. (2016), the present work has selected a few of their cases for more detailed analysis and three cases for high-resolution numerical simulation and sensitivity test to investigate the role played by the island of Sumatra in subsequent TC formation in the IO. The CReSS model employed has a convective-permitting 4-km grid size and large domain of 5600×4464 km^2 (Table 1), and the simulations for the three cases, including Nisha (2008) in NIO and the TC pairs of Ward and Cleo (2009), are for at least 15 days. In the CTL runs, the evolution of the vortices, including the lee stage (for Nisha and Ward), is reasonably well-captured. The results are then compared and contrasted to those in the sensitivity tests (NT runs), in which the topography of Sumatra is removed. The major findings of the present study can be summarized below.

1. In the NT tests without Sumatra topography, the three TC cases also all reach TS status as in the CTL experiment and observation, but tend to do so at a later time. This time

difference is 27 h for Nisha (2008), 12 h for Cleo (2009), and only 4 h and minimal for Ward (2009). The island of Sumatra therefore is not a necessary condition for TC genesis in the IO, as expected.

2. During the leeside stage of Nisha and Ward in NIO, both vortices in the CTL runs tend to possess a slightly stronger areal-mean vorticity in the low level compared to their counterpart in NT runs. A vorticity budget analysis indicates that the main contributing terms are vertical stretching and vertical transfer at the leeside. Thus, the Sumatra topography is still helpful in producing a larger vorticity and stronger initial vortex for subsequent development after vortex shedding.
3. For the four NIO cases examined, easterly or northeasterly winds near the northern tip of Sumatra, equatorial westerly wind surge, and advection of vorticity and moisture from upstream (either a TC/TS remnant or a BV) are common synoptic features at (or near) the formation of the lee vortex. A more extensive examination of 22 cases in October-December of 2008 and 2009 suggest that these favorable factors were also frequently present, especially in those that reached TS status in the Bay of Bangel. Evidently, these features and their associated environment lead to the intensification of the vortex in NT runs, from a (slightly) weaker vortex without Sumatra topography.
4. For Cleo (2009) in SIO, the formation area is not at lee but windward side due to the presence of equatorial westerly wind surge, as analyzed by Fine et al. (2016). The Sumatra topography in this case has a deflection effect on the westerly, and thereby provides stronger background vorticity (in combination with southeasterly wind farther south). As a result, the inner vortex in CTL remains stronger and reaches TS status earlier than its counterpart in the NT experiment.
5. A conceptual model is presented in Fig. 21, which summarizes the above results and depicts the favorable conditions for TC genesis in NIO from initial vortex from the

leeside of Sumatra as well as SIO. For NIO, these include northeasterly wind near 5°-10°N, equatorial WWB, and advection of vorticity/moisture from SCS. For SIO cases, they include the southward flow deflection of westerlies and southeasterly trade wind at higher latitudes.

Acknowledgements. The authors wish to thank Prof. C.-S. Lee of the National Taiwan University for his helpful comments. The ECMWF and YOTC project is acknowledged for making available the gridded analysis data. The TRMM PR/TMI observations in Figs. 7, 12, and 16 are provided by the NRL. This study is jointly supported by the Ministry of Science and Technology (MOST) of Taiwan under Grants MOST-105-2111-M-003-003-MY3, MOST-108-2111-M-003-005-MY2, and MOST-108-2625-M-003-001.

References

Chang, C.-P., C.-H. Liu and H.-C. Kuo, 2003: Typhoon Vamei: An equatorial tropical cyclone formation. *Geophys. Res. Lett.*, **30**, No. 3, 1150.

Chang, C.-P., P. A. Harr, and H. J. Chen, 2004: Synoptic disturbances over the equatorial South China Sea and western maritime continent during boreal winter. *Mon. Wea. Rev.*, **133**, 489–503.

Chen, Y.-H., H.-C. Kuo, C.-C. Wang, and Y.-T. Yang, 2017: Influence of southwest monsoon flow and typhoon track on Taiwan rainfall during the exit phase: Modeling study of Typhoon Morakot (2009). *Quart. J. Roy. Meteor. Soc.*, **143** (B), 3014–3024, doi: 10.1002/qj.3156.

Cotton, W. R., G. J. Tripoli, R. M. Rauber, and E. A. Mulvihill, 1986: Numerical simulation of the effects of varying ice crystal nucleation rates and aggregation processes on orographic snowfall. *J. Climate Appl. Meteor.*, **25**, 1658–1680.

Deardorff, J. W., 1980: Stratocumulus-capped mixed layers derived from a three-dimensional model. *Bound.-Layer Meteor.*, **18**, 495–527.

Emanuel, K. A., 1986: An air-sea interaction theory for tropical cyclones. Part I: Steady-state maintenance. *J. Atmos. Sci.*, **43**, 585–604.

Epifanio, C. C., 2003: Lee vortices. *Encyclopedia of Atmospheric Sciences*, J. R. Holton, J. Pyle, and J. A. Curry, Eds., Elsevier Science Ltd., 1150–1160.

Farfán, L. M., and J. A. Zehnder, 1997: Orographic influence on the synoptic-scale circulations associated with the genesis of Hurricane Guillermo (1991). *Mon. Wea. Rev*., **125**, 2683–2698.

Fine, C. M., R. H. Johnson, P. E. Ciesielski, and R. K. Taft, 2016: The role of topographically induced vortices in tropical cyclone formation over the Indian Ocean. *Mon. Wea. Rev.*, **127**, 4827–4847.

Gray, W. M., 1968: Global view of the origins of tropical disturbances and storms. *Mon. Wea. Rev.*, **96**, 669–700.

Ikawa, M., and K. Saito, 1991: Description of a nonhydrostatic model developed at the Forecast Research Department of the MRI. MRI Tech. Rep. 28, 238 pp.

Johnson, R. H., and P. E. Ciesielski, 2013: Structure and properties of Madden–Julian oscillations deduced from DYNAMO sounding arrays. *J. Atmos. Sci.*, **70**, 3157–3179, doi:10.1175/JAS-D-13-065.1.

Kikuchi, K., and B. Wang, 2010: Formation of tropical cyclones in the northern Indian Ocean associated with two types of tropical intraseasonal oscillation modes. *J. Meteor. Soc. Japan*, **88**, 475–196.

Kondo, J., 1976: Heat balance of the China Sea during the air mass transformation experiment. *J. Meteor. Soc. Japan*, **54**, 382–398.

Kuettner, J. P., 1967: The equatorial double vortex: Unique hydrodynamic role of Sumatra in atmospheric developments over the Indian Ocean. *Bull. Amer. Meteor. Soc.*, **48**, 637.

Kuettner, J. P., 1989: Easterly flow over the cross equatorial island of Sumatra and its role in the formation of cyclone pairs over the Indian Ocean. *Wetter Leben*, **4**, 47–55.

Kuo, H.-C., S. Tsujino, C.-C. Huang, C.-C. Wang, and K. Tsuboki, 2019: Diagnosis of the dynamic efficiency of latent heat release and the rapid intensification of Supertyphoon Haiyan (2013). *Mon. Wea. Rev.*, **147**, 1127–1147, doi: 10.1175/ MWR-D-18-0149.1.

Lee, C.-S., 1986: An observational study of tropical cloud cluster evolution and cyclogenesis in the western North Pacific. Dept. of Atmos. Sci. Paper No. 403, Colo. State Univ., Ft. Collins, CO, 250 pp.

Lee, C.-S., R. Edson, and W. M. Gray, 1989: Some large-scale characteristics associated with tropical cyclone development in the North Indian Ocean during FGGE. *Mon. Wea. Rev.*, **117**, 407–426.

Lin, Y.-L., and C.-S. Lee, 2011: An analysis of tropical cyclone formations in the South China Sea during the late season. *Mon. Wea. Rev.*, **139**, 2748–2760.

Lin, Y.-L., R. D. Farley, and H. D. Orville, 1983: Bulk parameterization of the snow field in a cloud model. *J. Climate Appl. Meteor.*, **22**, 1065–1092.

Louis, J. F., M. Tiedtke, and J. F. Geleyn, 1982: A short history of the operational PBL parameterization at ECMWF. *Workshop on Planetary Boundary Layer Parameterization*, 25-27 November 1981, Reading, UK, 59–79.

Love, G., 1985a: Cross-equatorial influence of winter hemisphere subtropical cold surges. *Mon. Wea. Rev.*, **113**, 1487–1498.

Love, G., 1985b: Cross-equatorial interaction during tropical cyclone genesis. *Mon. Wea. Rev.*, **113**, 1499–1509.

Moncrieff, M.W., 2010: The multiscale organization of moist convection and the intersection of weather and climate. *Why Does Climate Vary?*, *Geophys. Monogr.*, Vol. 189, Amer. Geophys. Union, 3–26.

Moncrieff, M. W., D. E. Waliser, M. J. Miller, M. A. Shapiro, G. R. Asrar, and J. Caughey, 2012: Multiscale convective organization and the YOTC virtual global field campaign. *Bull. Amer. Meteor. Soc.*, **93**, 1171–1187, doi:10.1175/BAMS-D-11-00233.1.

Mozer, J. B., and J. A. Zehnder, 1996: Lee vorticity production by large-scale tropical mountain ranges. Part I: A mechanism for tropical cyclogenesis in the eastern North Pacific. *J. Atmos. Sci.*, **53**, 521–538.

Murakami, M., 1990: Numerical modeling of dynamical and microphysical evolution of an isolated convective cloud---The 19 July 1981 CCOPE cloud. *J. Meteor. Soc. Japan*, **68**, 107–128.

Murakami, M., T. L. Clark, and W. D. Hall, 1994: Numerical simulations of convective snow clouds over the Sea of Japan: Two-dimensional simulation of mixed layer development

and convective snow cloud formation. *J. Meteor. Soc. Japan*, **72**, 43–62.

Ooyama, K. V., 1982: Conceptual evolution of the theory and modeling of the tropical cyclone. *J. Meteor. Soc. Japan*, **60**, 369–379.

Ritchie, E. A., and G. J. Holland, 1999: Large-scale patterns associated with tropical cyclogenesis in the western Pacific. *Mon. Wea. Rev.*, **127**, 2027–2043.

Rotunno, R., and K. A. Emanuel, 1987: An air-sea interaction theory for tropical cyclones. Part II: Evolutionary study using a nonhydrostatic axisymmetric numerical model. *J. Atmos. Sci.*, **44**, 542–561.

Rotunno, R., and P. K., Smolarkiewicz, 1991: Further results on lee vortices in low-Froude-number flow. *J. Atmos. Sci.*, **48**, 2204–2211.

Rydbeck, A. V., E. C. Maloney, and G. J. Alaka, Jr., 2017: In situ initiation of East Pacific easterly waves in a regional model. *J. Atmos. Sci.*, **74**, 333–351.

Segami, A., K. Kurihara, H. Nakamura, M. Ueno, I. Takano, and Y. Tatsumi, 1989: Operational mesoscale weather prediction with Japan Spectral Model. *J. Meteor. Soc. Japan*, **64**, 637–664.

Subbaramayya, I., and S. R. M. Rao, 1984: Frequency of Bay of Bengal cyclones in the post-monsoon season. *Mon. Wea. Rev.*, **112**, 1640–1642.

Smolarkiewicz, P. K., and R. Rotunno, 1989: Low Froude number flow past three-dimensional obstacles. Part I: Baroclinically generated lee vortices. *J. Atmos. Sci.*, **46**, 1154–1164.

Takahashi, H. G., Y. Fukutomi, and J. Matsumoto, 2011: The impact of long-lasting northerly surges of the East Asian winter monsoon on tropical cyclogenesisand its seasonal march. *J. Meteor. Soc. Japan*, **89A**, 181–200.

Tsuboki, K., and A. Sakakibara, 2002: Large-scale parallel computing of cloud resolving storm simulator. *High Performance Computing*, Springer, H. P. Zima et al. Eds.,

243–259.

Tsuboki, K., and A. Sakakibara, 2007: *Numerical Prediction of High-Impact Weather Systems. The Textbook for the Seventeenth IHP Training Course in 2007.* Hydrospheric Atmospheric Research Center, Nagoya University and UNESCO, 273 pp.

Waliser, D. E., and Coauthors, 2012: The ‘‘Year’’ of Tropical Convection (May 2008–April 2010): Climate variability and weather highlights. B*ull. Amer. Meteor. Soc.*, **93**, 1189–1218, doi:10.1175/2011BAMS3095.1.

Wang, B., and J.-Y. Moon, 2017: An anomalous genesis potential index for MJO modulation of tropical cyclones. *J. Climate*, **17**, 4021–4035.

Wang, C.-C., 2015: The more rain, the better the model performs—The dependency of quantitative precipitation forecast skill on rainfall amount for typhoons in Taiwan. *Mon. Wea. Rev.*, **143**, 1723–1748, doi:10.1175/MWR-D-14-00137.1.

Wang, C.-C., H.-C. Kuo, Y.-H. Chen, H.-L. Huang, C.-H. Chung, and K. Tsuboki, 2012: Effects of asymmetric latent heating on typhoon movement crossing Taiwan: The case of Morakot (2009) with extreme rainfall. *J. Atmos. Sci.*, **69**, 3172–3196.

Wang, C.-C., Y.-H. Chen, H.-C. Kuo, and S.-Y. Huang, 2013: Sensitivity of typhoon track to asymmetric latent heating/rainfall induced by Taiwan topography: A numerical study of Typhoon Fanapi (2010). *J. Geophys. Res.*, **118**(D8), 3292–3308, doi:10.1002/jgrd.50351.

Wang, C.-C., H.-C. Kuo, R. H. Johnson, C.-Y. Lee, S.-Y. Huang, and Y.-H. Chen, 2015: A numerical study of convection in rainbands of Typhoon Morakot (2009) with extreme rainfall: Roles of pressure perturbations with low-level wind maxima. *Atmos. Chem. Phys.*, **15**, 11097–11115, doi:10.5194/acp-15-11097-2015.

Wang, C.-C., S.-Y. Huang, S.-H. Chen, C.-S. Chang, and K. Tsuboki, 2016: Cloud-resolving typhoon rainfall ensemble forecasts for Taiwan with large domain and extended range through time-lagged approach. *Wea. Forecasting*, **31**, 151–172.

Zehnder, J. A., D. M. Powell, and D. L. Ropp, 1999: The interaction of easterly waves, orography, and the intertropical convergence zone in the genesis of eastern Pacific tropical cyclones. *Mon. Wea. Rev.*, **127**, 1566–1585.

Figure caption

FIG. 1. (a) The topography of Sumatra and surrounding region (m, color), and a schematic of lee vortices based on Kuettner (1967). The gray-dotted polygon shows the area to remove terrain in sensitivity tests, and the red-dotted line shows the segment used to compute Fr. (b) Tracks of the five selected cases (see insert, thickened for lifespan reaching TS intensity) and the model simulation domain (thick solid box).

FIG. 2. Time-height section of mean relative vorticity (ζ, 10^{-6} s^{-1}), computed from ECMWF-YOTC data and averaged inside 550 km from the vortex center, for the four cases in NIO: (a) 03A, (b) Nisha, (c) 07B, and (d) Ward. Each panel starts at the time of lee vortex formation. The thick dashed vertical lines mark the time when the vortex started to shed (as labeled), and the gray dashed horizontal lines depict the level of maximum vorticity.

FIG. 3. Distributions of horizontal wind (gray vectors, m s^{-1}) and relative vorticity (10^{-5} s^{-1}, color, cyclonic only) in ECMWF-YOTC data two days before (left), at the time (middle) of, and two days after (right) the formation of the lee vortex for (a) 03A at 850 hPa, (b) Nisha at 700 hPa, (c) 07B at 500 hPa, and (d) Ward at 600 hPa. The vortex centers are marked by a green “x”, and both the reference vector and color scales are plotted at the bottom.

FIG. 4. Longitude-time (Hovmoller) diagrams of mean (a)-(d) relative vorticity (10^{-5} s^{-1}) at the pressure level as labeled (same as in Fig. 3) and (e)-(h) total column-integrated precipitable water (mm) in ECMWF-YOTC data during the case period of 03A, Nisha, 07B, and Ward, respectively (from top to bottom). The latitudinal range of averaging is 0°-15°N. The circles depict the time of lee vortex formation, and the vertical dashed lines mark the boundary between the IO and the SCS (near 100°E).

FIG. 5. Distribution of total column-integrated precipitable water (mm, color) and horizontal

wind at 925 hPa (m s^{-1}, gray vectors) at the time of lee vortex formation for (a) 03A, (b) Nisha, (c) 07B, and (d) Ward, respectively. The vortex centers (at 850 hPa) are marked by an "x". The red dashed circles depict TC or TD in the IO, green dashed circles depict TD or pre-TC in SIO, and white dashed circles depict BV or TC ranment in the SCS. Both the reference vector and color scales are plotted at the bottom.

FIG. 6. Comparison of (a) track, (b) maximum surface wind speed (kts, at 10-m height), and (c) central mean sea-level pressure (hPa) among JTWC best track, ECMWF-YOTC, and CTL and NT experiments for the case of Nisha (16 to 28 Nov 2008). The vortex center positions are given by small dots every 6 h, median dots at 0000 UTC, and large dots every three days with dates labeled (unless not necessary) in (a). Track endpoints are also labeled (with time if not at 0000 UTC). In (b), TS intensity (34 kts) and the time to reach it in the four data sources are marked.

FIG. 7. (a)-(d) SSMI 91-GHz imagery of brightness temperature (T_B, K, color), overlaid on METEO-7 infrared (IR) cloud image (gray shades), of Nisha at (a) 1415 UTC Nov 25, (b) 0021 and (c) 1403 UTC 26 Nov, and (d) 0008 UTC 27 Nov 2008 (source: NRL). (e)-(h) Column maximum mixing ratio of precipition (g kg^{-1}, rain + snow + graupel) and horizontal wind at 850 hPa (kts, white barbs) in CTL at full hours closest to (a)-(d) as labeled, respectively. The color scales are plotted at the bottom.

FIG. 8. Time-height section of mean relative vorticity (ζ, 10^{-6} s^{-1}) for Nisha similar to Fig. 2b, except from (a) CTL and (b) NT experiment, and (c) their difference (CTL – NT). Downward developments during the lee stage are marked.

FIG. 9. The vorticity-tendency budget terms (10^{-9} s^{-2}, left axis), including local tendency, horizontal advection, vertical advection, convergence, tilting, solenoidal, and residual terms (see legend), and the mean vorticity (10^{-5} s^{-1}, dashed, right axis) at the height of 1547 m, averaged inside 550 km, for Nisha from 1200 UTC 15 Nov to 0000 UTC 18

Nov 2008 in (a) CTL and (b) NT experiment.

FIG. 10. The correlation coefficients between *Fr* and lagged mean vorticity tendency (as in Figs. 9 and 14), as a function of lagged time (h) in CTL and NT experiments for the case of (a) Nisha and (b) Ward, respectively.

FIG. 11. FIG. 11. As in Fig. 6, except for the case of TC Ward (30 Nov to 16 Dec 2009).

FIG. 12. As in Fig. 7, except for Ward at (a) 0158 and (b) 1307 UTC 11 Dec, and (c) 0146 and (d) 1157 UTC 12 Dec 2009 (source: NRL), and (e)-(h) from CTL at full hours closest to (a)-(d) as labeled, respectively.

FIG. 13. As in Fig. 8, except for the case of TC Ward.

FIG. 14. As in Fig. 9, except for Ward from 0000 UTC 30 Nov to 0000 UTC 3 Dec 2009.

FIG. 15. As in Fig. 6, except for the case of TC Cleo (29 Nov to 10 Dec 2009).

FIG. 16. As in Fig. 7, except for Cleo at (a) 1405 UTC 6 Dec, and (b) 0016 and (c) 1353 UTC 7 Dec 2009 (source: NRL), and (d)-(f) from CTL at full hours closest to (a)-(c) as labeled, respectively.

FIG. 17. As in Fig. 8, except for the case of TC Cleo.

FIG. 18. As in Fig. 9, except for Cleo from 0000 UTC 1 Dec to 0000 UTC 4 Dec 2009. Note that the vertical scale is reversed for this case in the Southern Hemisphere.

FIG. 19. Averaged low-level horizontal wind (m s^{-1}, over 50-1913 m) in the northeastern quadrant of Cleo at 1-h intervals from 0000 UTC 1 Dec to 0000 UTC 4 Dec 2009 in CTL and NT experiments.

FIG. 20. Time-series of westerly wind speed in equatorial IO (kts, red, averaged over 5°S-5°N, 80°-90°E) and northeasterly wind speed east of northern Sumatra (kts, blue, averaged over 5°-10°N, 107°-115°E) at 925 hPa in the ECMWF-YOTC data during Oct-Dec of (a) 2008 and (b) 2009. Black/gray segments indicate periods with closed vortex in BOB/AS (divided at 80°E) with named storms labeled (the naming times shown by short red ticks).

The periods with 700-hPa positive vorticity advection (pink) and moisture advection (orange) at the SCS are also marked.

FIG. 21. Schematics for synoptic conditions favorable for the formation of lee vortices to the west of Sumatra that may subsequently develop into TCs in the IO during the post-monsoon period (Oct-Dec), obtained in this study. These factors include vorticity and moisture advection from the SCS (linked to TC remnant or BV), prevailing northeasterly (southeasterly) winds in NH (SH), and the deflection of low-level northeasterly wind by the northern part (westerly wind by the southern part) of Sumatra for the northern (southern) vortex.

TABLE 1. The CReSS model domain configuration (top), initial and boundary conditions (IC/BCs, middle), and physical schemes (bottom) used in this study.

Cases	Nisha (2008)	Ward and Cleo (2009)
Projection	Mercater, center at 100°E	
Grid spacing (km)	4.0 × 4.0 × 0.1-0.727 (0.5)*	
Grid dimension (x, y, z) and domain size (km)	1400 × 1116 × 40 (5600 × 4464 × 20)	
IC/BCs (including SST)	ECMWF-YOTC analyses (0.25°, 20 levels, every 6 h)	
Topography	Digital elevation model at (1/120)°	
Initial time	1200 UTC 14 Nov 2008	0000 UTC 29 Nov 2009
Integration length	15 days	16 days
Output frequency	1 h	
Cloud microphysics	Bulk cold-rain (Lin et al. 1983; Cotton et al. 1986; Murakami 1990; Ikawa and Saito 1991; Murakami et al. 1994)	
PBL/turbulence	1.5-order closure with prediction of turbulent kinetic energy (Deardorff 1980; Tsuboki and Sakakibara 2007)	
Surface processes	Energy/momentum fluxes, shortwave and longwave radiation (Kondo 1976; Louis et al. 1982; Segami et al. 1989)	
Substrate model	43 levels, every 5 cm to 2.1 m	

* The vertical grid spacing (Δz) of CReSS is stretched (smallest at the bottom), and the averaged spacing is given in the parentheses.

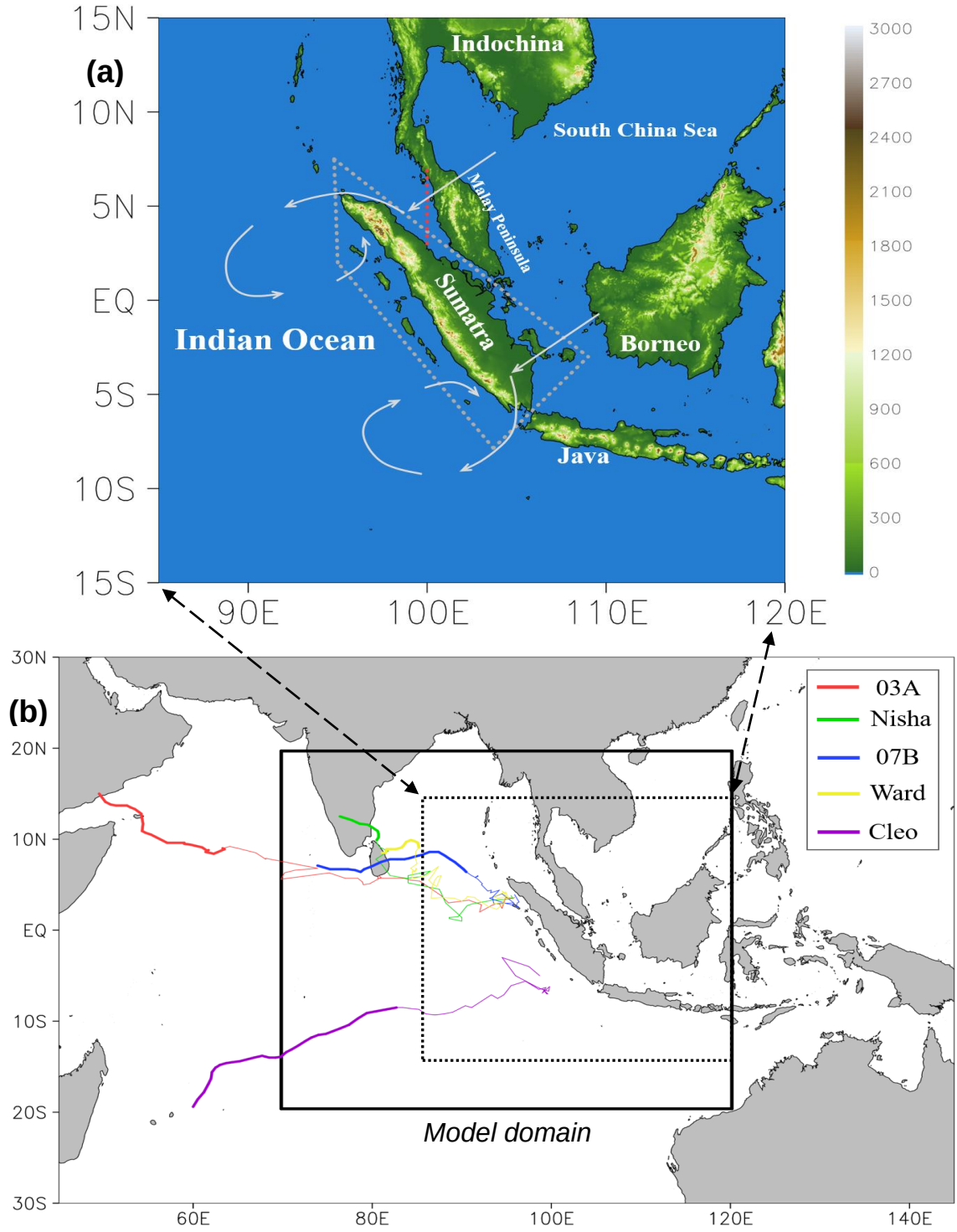

1 FIG. 1. (a) The topography of Sumatra and surrounding region (m, color), and a schematic of
2 lee vortices based on Kuettner (1967). The gray-dotted polygon shows the area to
3 remove terrain in sensitivity tests, and the red-dotted line shows the segment used to
4 compute Fr. (b) Tracks of the five selected cases (see insert, thickened for lifespan
5 reaching TS intensity) and the model simulation domain (thick solid box).

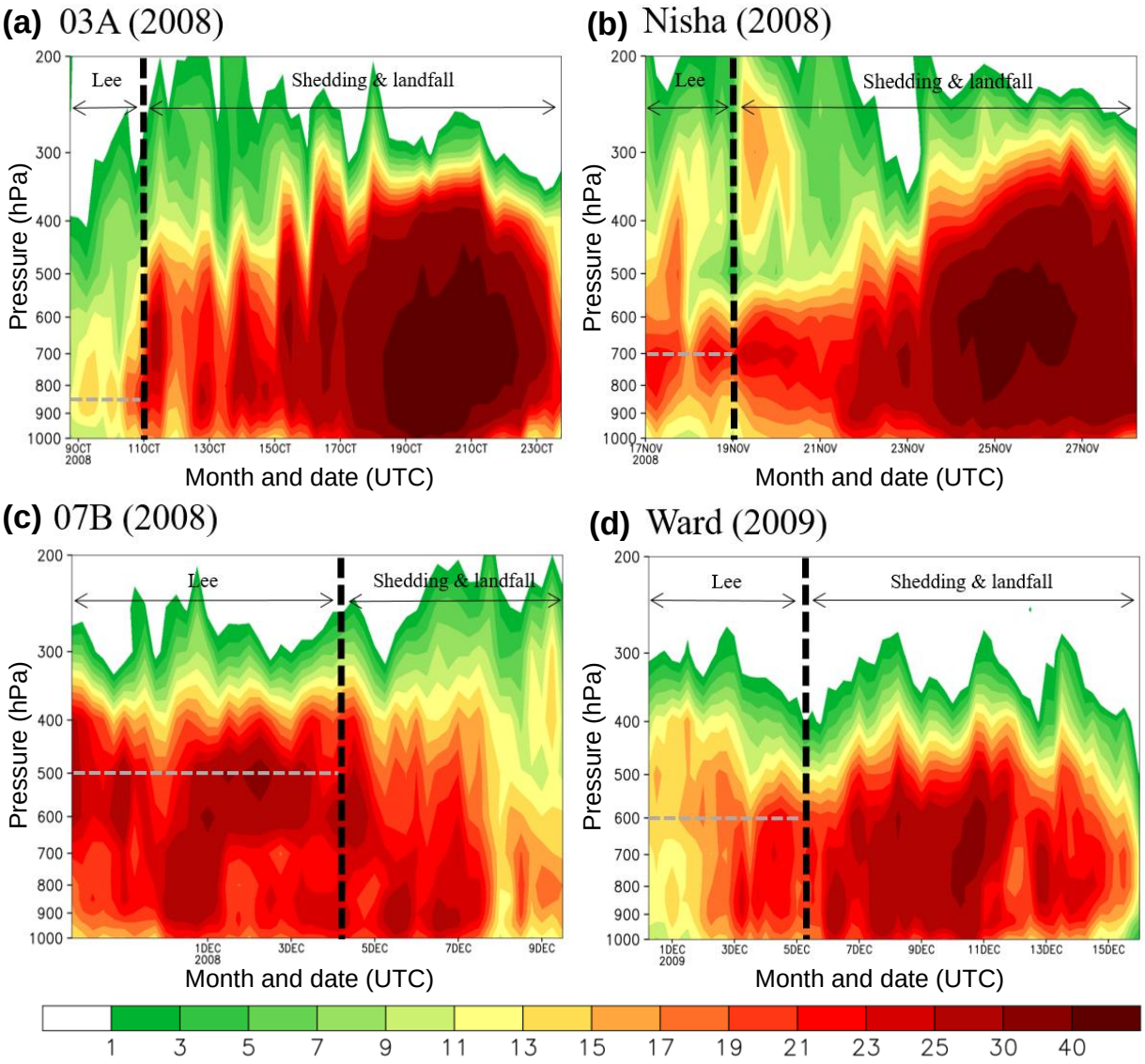

1 FIG. 2. Time-height section of mean relative vorticity (ζ, 10^{-6} s^{-1}), computed from
2 ECMWF-YOTC data and averaged inside 550 km from the vortex center, for the four
3 cases in NIO: (a) 03A, (b) Nisha, (c) 07B, and (d) Ward. Each panel starts at the time of
4 lee vortex formation. The thick dashed vertical lines mark the time when the vortex
5 started to shed (as labeled), and the gray dashed horizontal lines depict the level of
6 maximum vorticity.

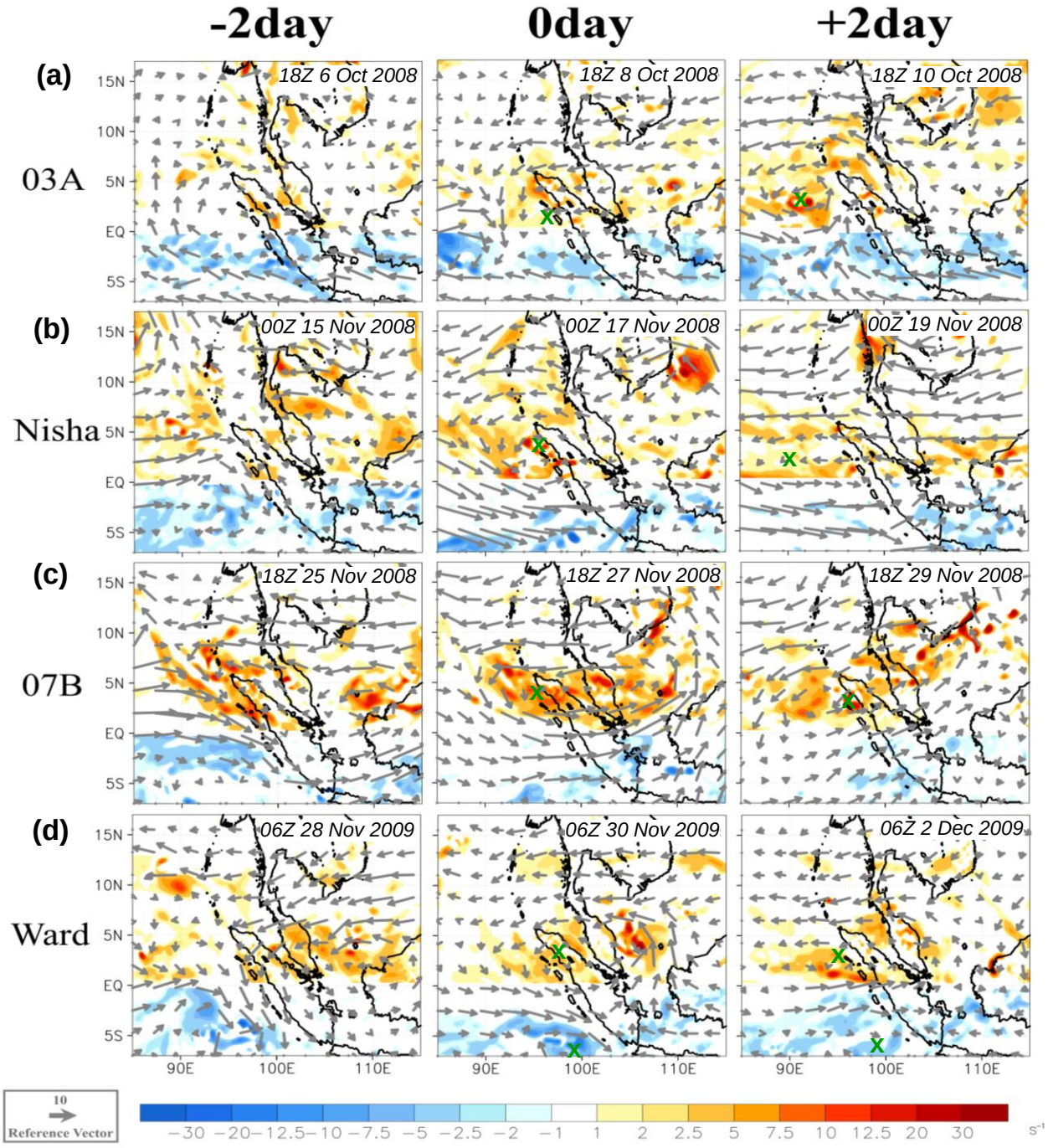

1 FIG. 3. Distributions of horizontal wind (gray vectors, m s^{-1}) and relative vorticity (10^{-5} s^{-1},
2 color, cyclonic only) in ECMWF-YOTC data two days before (left), at the time (middle)
3 of, and two days after (right) the formation of the lee vortex for (a) 03A at 850 hPa, (b)
4 Nisha at 700 hPa, (c) 07B at 500 hPa, and (d) Ward at 600 hPa. The vortex centers are
5 marked by a green "x", and both the reference vector and color scales are plotted at the
6 bottom.

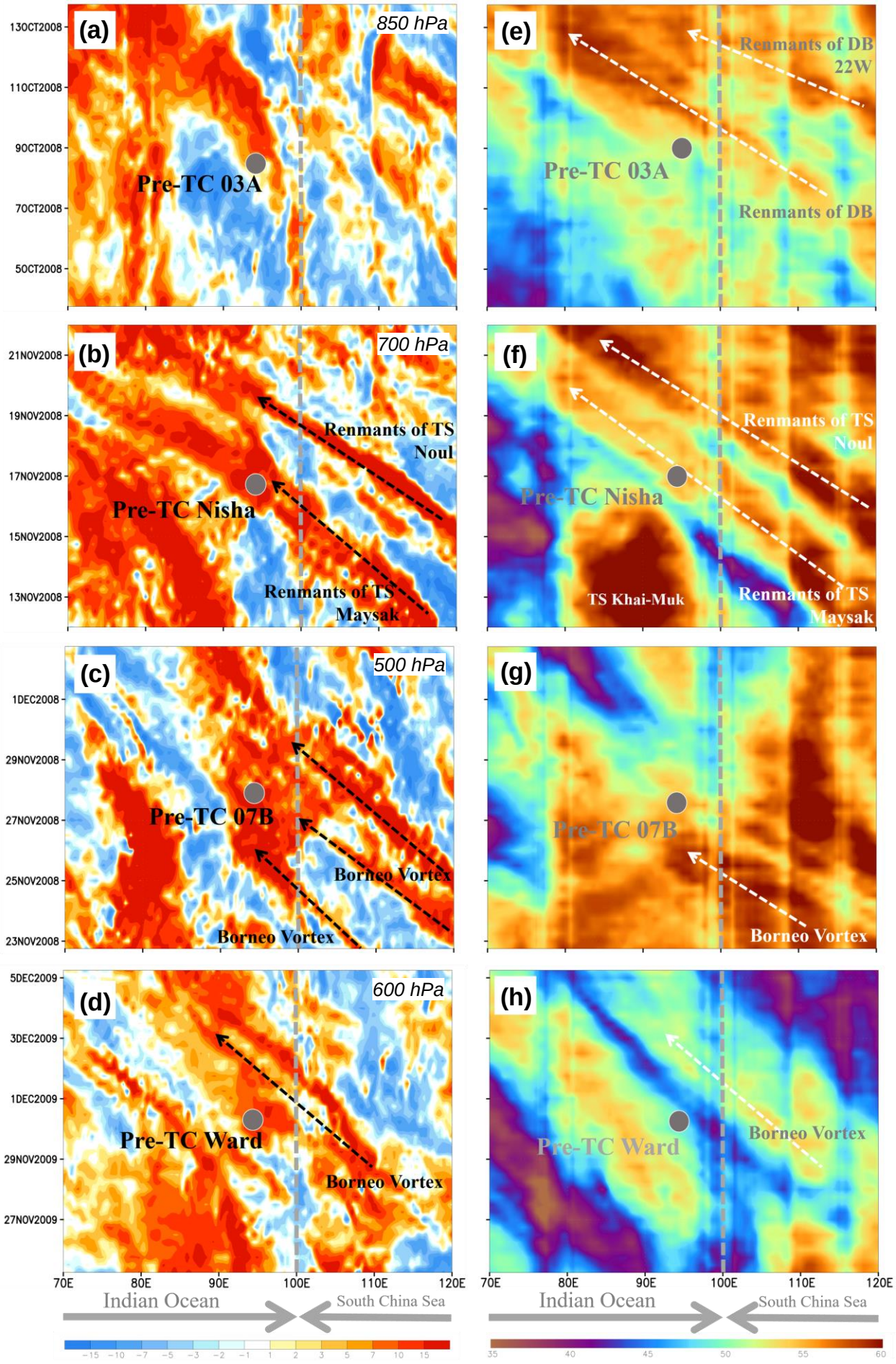
(a)
850 hPa
Pre-TC 03A
13OCT2008
11OCT2008
9OCT2008
7OCT2008
5OCT2008
(e)
Renmants of DB
22W
Pre-TC 03A
Renmants of DB
(b)
700 hPa
Renmants of TS
Noul
Pre-TC Nisha
Renmants of TS
Maysak
21NOV2008
19NOV2008
17NOV2008
15NOV2008
13NOV2008
(f)
Renmants of TS
Noul
Pre-TC Nisha
TS Khai-Muk
Renmants of TS
Maysak
(c)
500 hPa
Pre-TC 07B
Borneo Vortex
Borneo Vortex
1DEC2008
29NOV2008
27NOV2008
25NOV2008
23NOV2008
(g)
Pre-TC 07B
Borneo Vortex
(d)
600 hPa
Pre-TC Ward
Borneo Vortex
5DEC2009
3DEC2009
1DEC2009
29NOV2009
27NOV2009
(h)
Pre-TC Ward
Borneo Vortex
70E
80E
90E
100E
110E
120E
Indian Ocean
South China Sea
−15 −10 −7 −5 −3 −2 −1 1 2 3 5 7 10 15
35 40 45 50 55 60

FIG. 4. Longitude-time (Hovmoller) diagrams of mean (a)-(d) relative vorticity (10^{-5} s^{-1}) at the pressure level as labeled (same as in Fig. 3) and (e)-(h) total column-integrated precipitable water (mm) in ECMWF-YOTC data during the case period of 03A, Nisha, 07B, and Ward, respectively (from top to bottom). The latitudinal range of averaging is 0°-15°N. The circles depict the time of lee vortex formation, and the vertical dashed lines mark the boundary between the IO and the SCS (near 100°E).

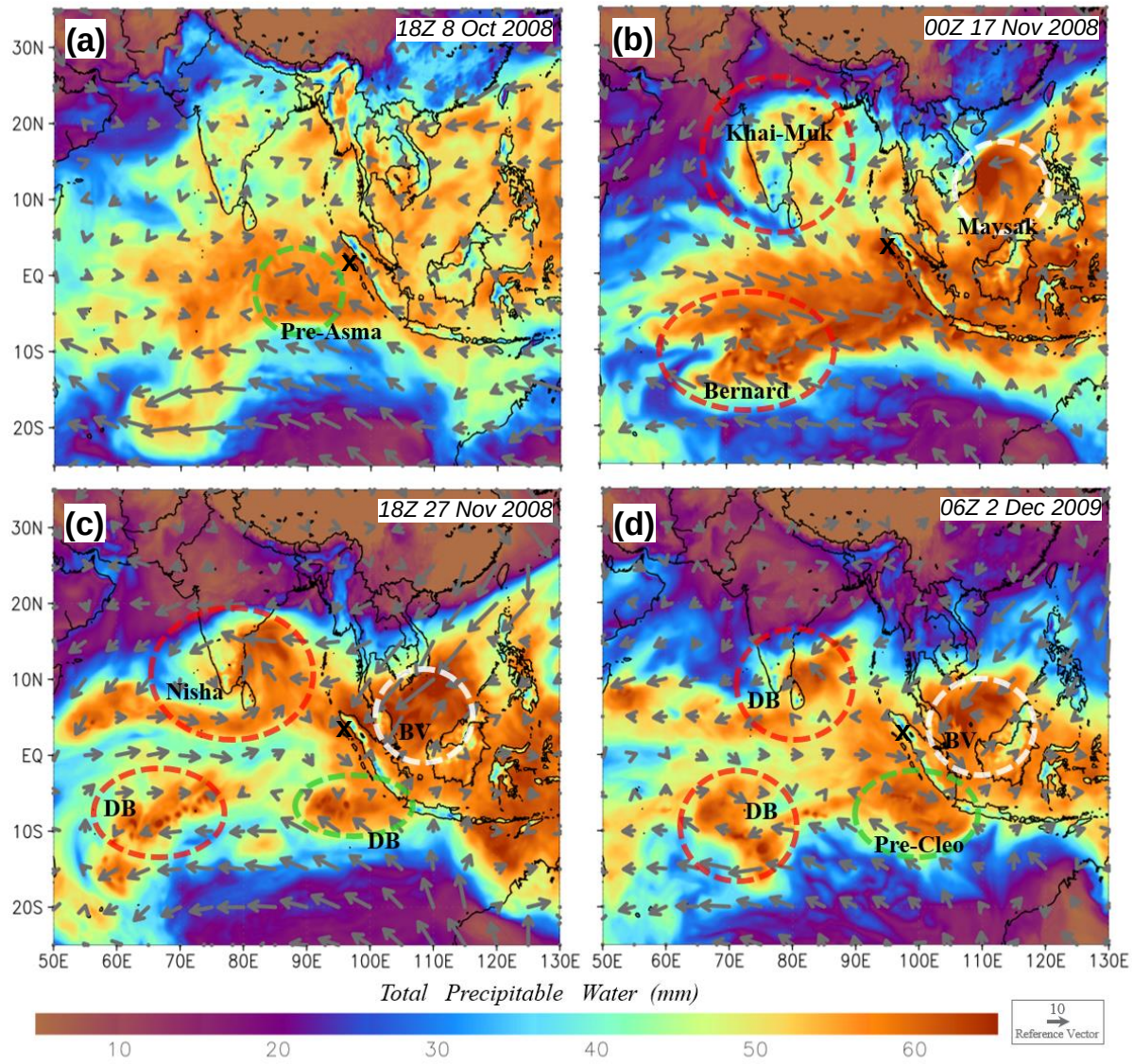

1 FIG. 5. Distribution of total column-integrated precipitable water (mm, color) and horizontal
2 wind at 925 hPa (m s^{-1}, gray vectors) at the time of lee vortex formation for (a) 03A, (b)
3 Nisha, (c) 07B, and (d) Ward, respectively. The vortex centers (at 850 hPa) are marked
4 by an "x". The red dashed circles depict TC or TD in the IO, green dashed circles depict
5 TD or pre-TC in SIO, and white dashed circles depict BV or TC ranment in the SCS.
6 Both the reference vector and color scales are plotted at the bottom.

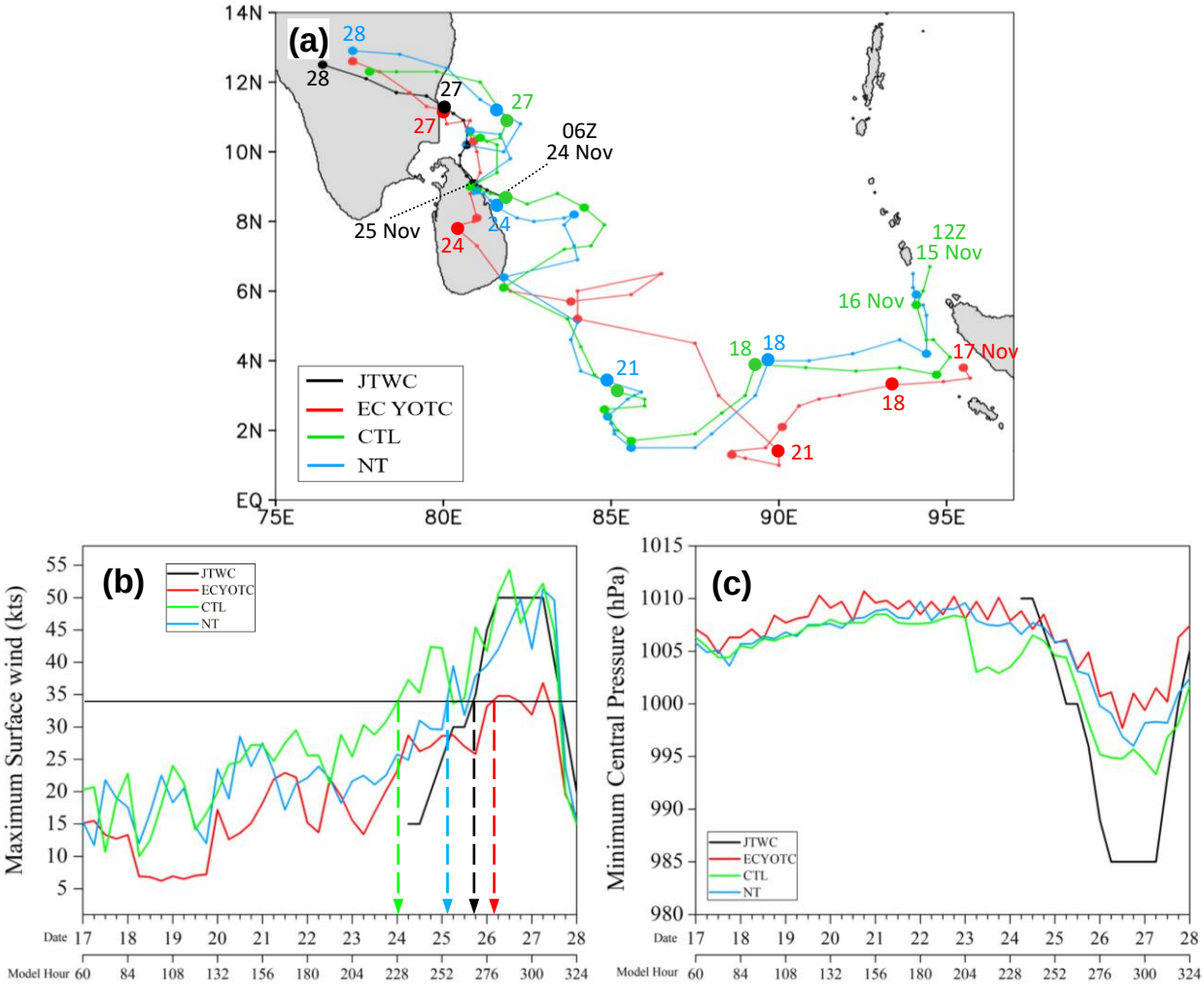

1 FIG. 6. Comparison of (a) track, (b) maximum surface wind speed (kts, at 10-m height), and
2 (c) central mean sea-level pressure (hPa) among JTWC best track, ECMWF-YOTC, and
3 CTL and NT experiments for the case of Nisha (16 to 28 Nov 2008). The vortex center
4 positions are given by small dots every 6 h, median dots at 0000 UTC, and large dots
5 every three days with dates labeled (unless not necessary) in (a). Track endpoints are also
6 labeled (with time if not at 0000 UTC). In (b), TS intensity (34 kts) and the time to reach
7 it in the four data sources are marked.

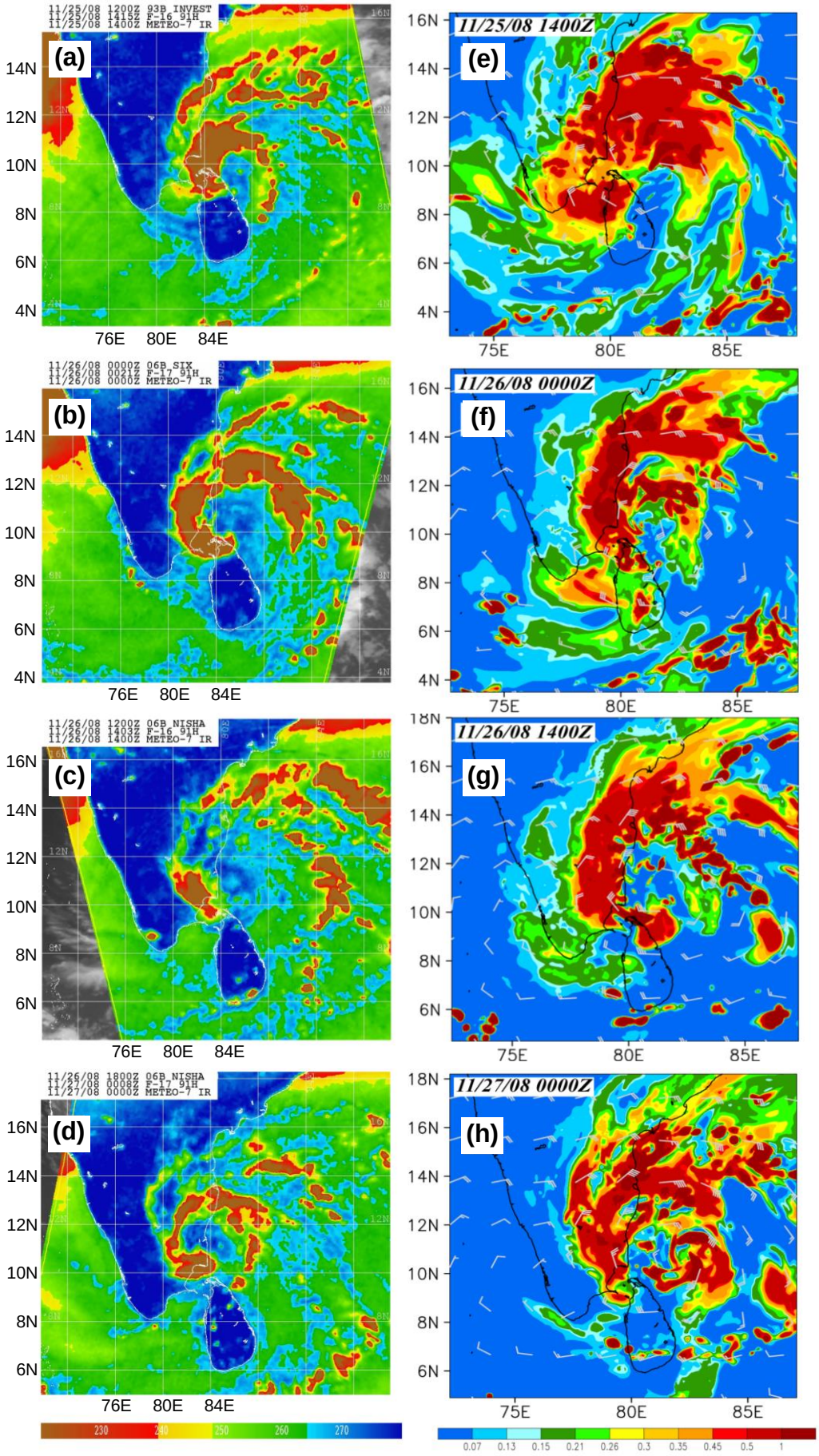
11/25/08 1200Z 03B INVEST
11/26/08 1415Z F-16 91H
11/25/08 1400Z METEO-7 IR
(a)
11/26/08 0000Z 06B SIX
11/26/08 0021Z F-17 91H
11/26/08 0000Z METEO-7 IR
(b)
11/26/08 1200Z 06B NISHA
11/26/08 1403Z F-16 91H
11/26/08 1400Z METEO-7 IR
(c)
11/26/08 1800Z 06B NISHA
11/27/08 0008Z F-17 91H
11/27/08 0000Z METEO-7 IR
(d)
16N
14N
12N
10N
8N
6N
4N
76E
80E
84E
230
240
250
260
270
11/25/08 1400Z
(e)
11/26/08 0000Z
(f)
11/26/08 1400Z
(g)
11/27/08 0000Z
(h)
18N
75E
85E
0.07
0.13
0.15
0.21
0.26
0.3
0.35
0.45
0.5
1

FIG. 7. (a)-(d) SSMI 91-GHz imagery of brightness temperature (T_B, K, color), overlaid on METEO-7 infrared (IR) cloud image (gray shades), of Nisha at (a) 1415 UTC Nov 25, (b) 0021 and (c) 1403 UTC 26 Nov, and (d) 0008 UTC 27 Nov 2008 (source: NRL). (e)-(h) Column maximum mixing ratio of precipition (g kg^{-1}, rain + snow + graupel) and horizontal wind at 850 hPa (kts, white barbs) in CTL at full hours closest to (a)-(d) as labeled, respectively. The color scales are plotted at the bottom.

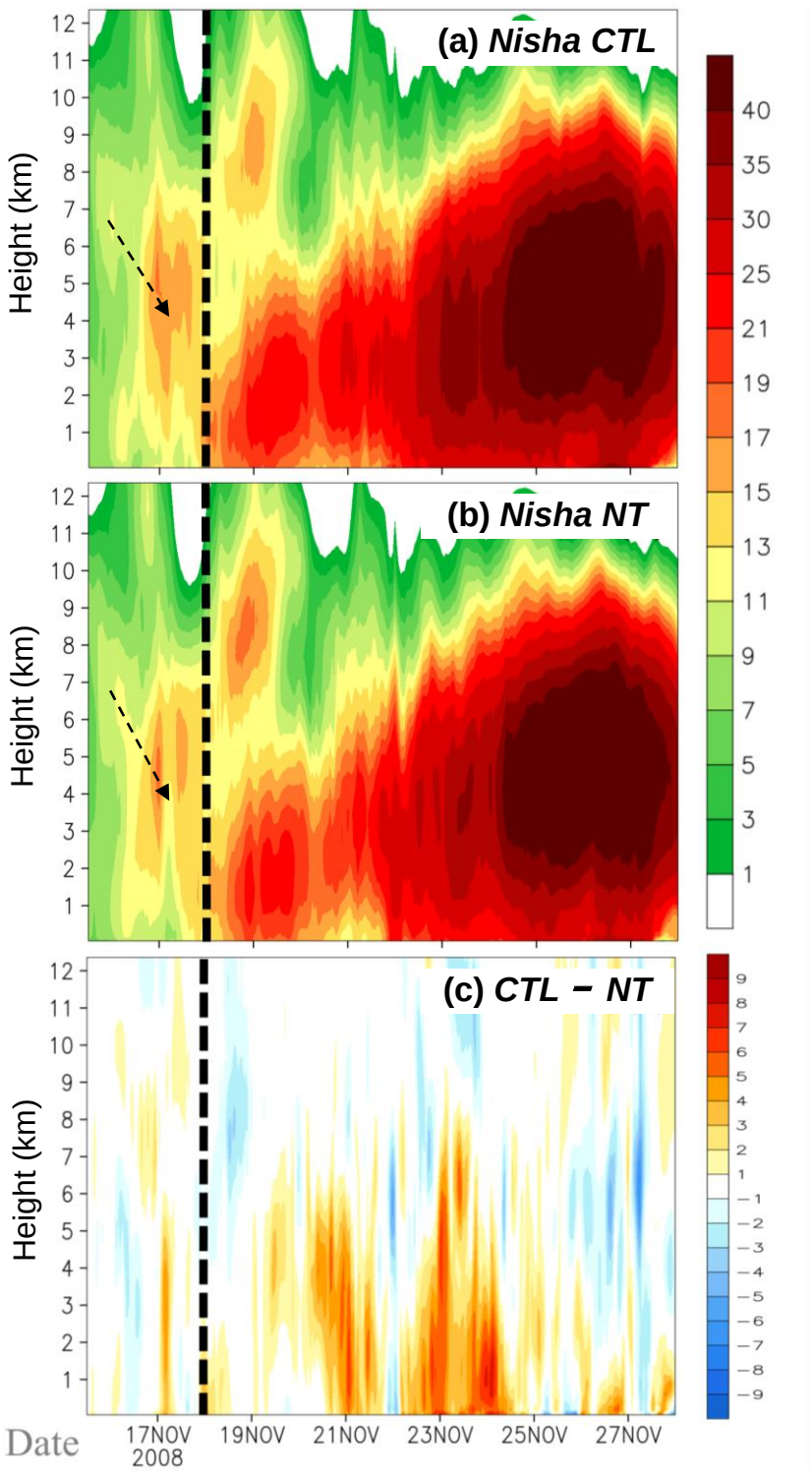

1 FIG. 8. Time-height section of mean relative vorticity (ζ, 10^{-6} s^{-1}) for Nisha similar to Fig. 2b,
2 except from (a) CTL and (b) NT experiment, and (c) their difference (CTL – NT).
3 Downward developments during the lee stage are marked.

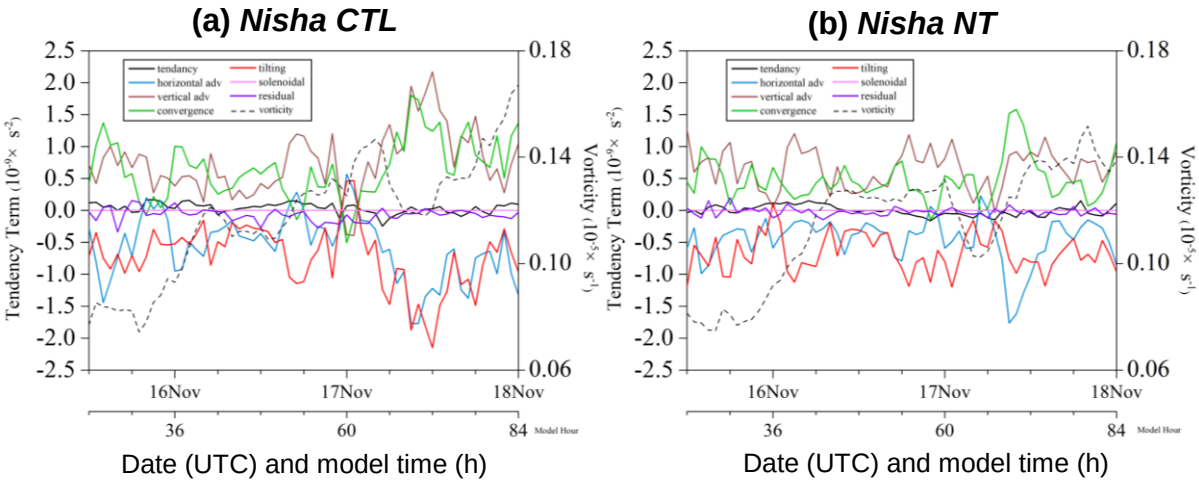

1 FIG. 9. The vorticity-tendency budget terms (10^{-9} s^{-2}, left axis), including local tendency,
2 horizontal advection, vertical advection, convergence, tilting, solenoidal, and residual
3 terms (see legend), and the mean vorticity (10^{-5} s^{-1}, dashed, right axis) at the height of
4 1547 m, averaged inside 550 km, for Nisha from 1200 UTC 15 Nov to 0000 UTC 18
5 Nov 2008 in (a) CTL and (b) NT experiment.

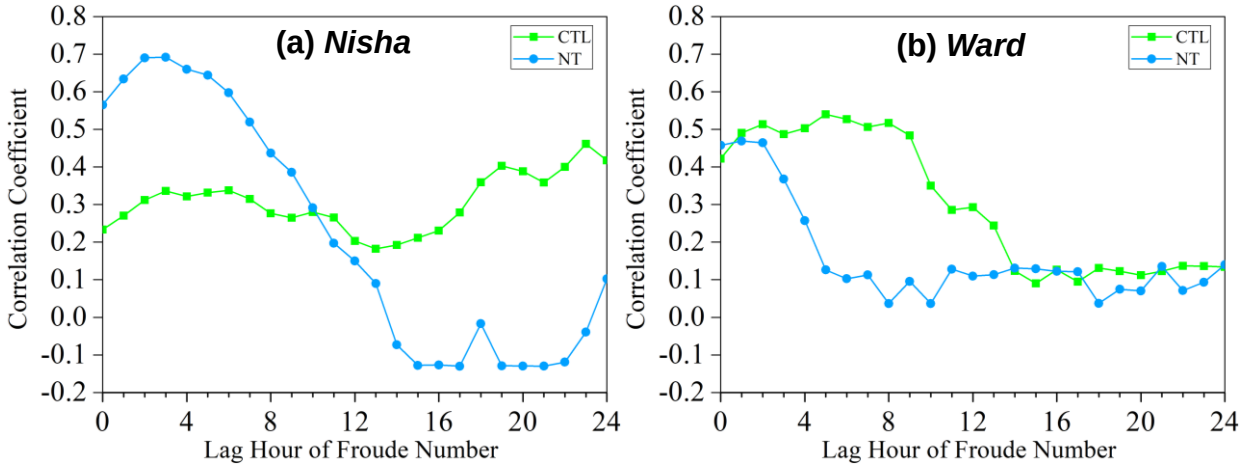

1 FIG. 10. The correlation coefficients between *Fr* and lagged mean vorticity tendency (as in
2 Figs. 9 and 14), as a function of lagged time (h) in CTL and NT experiments for the case
3 of (a) Nisha and (b) Ward, respectively.

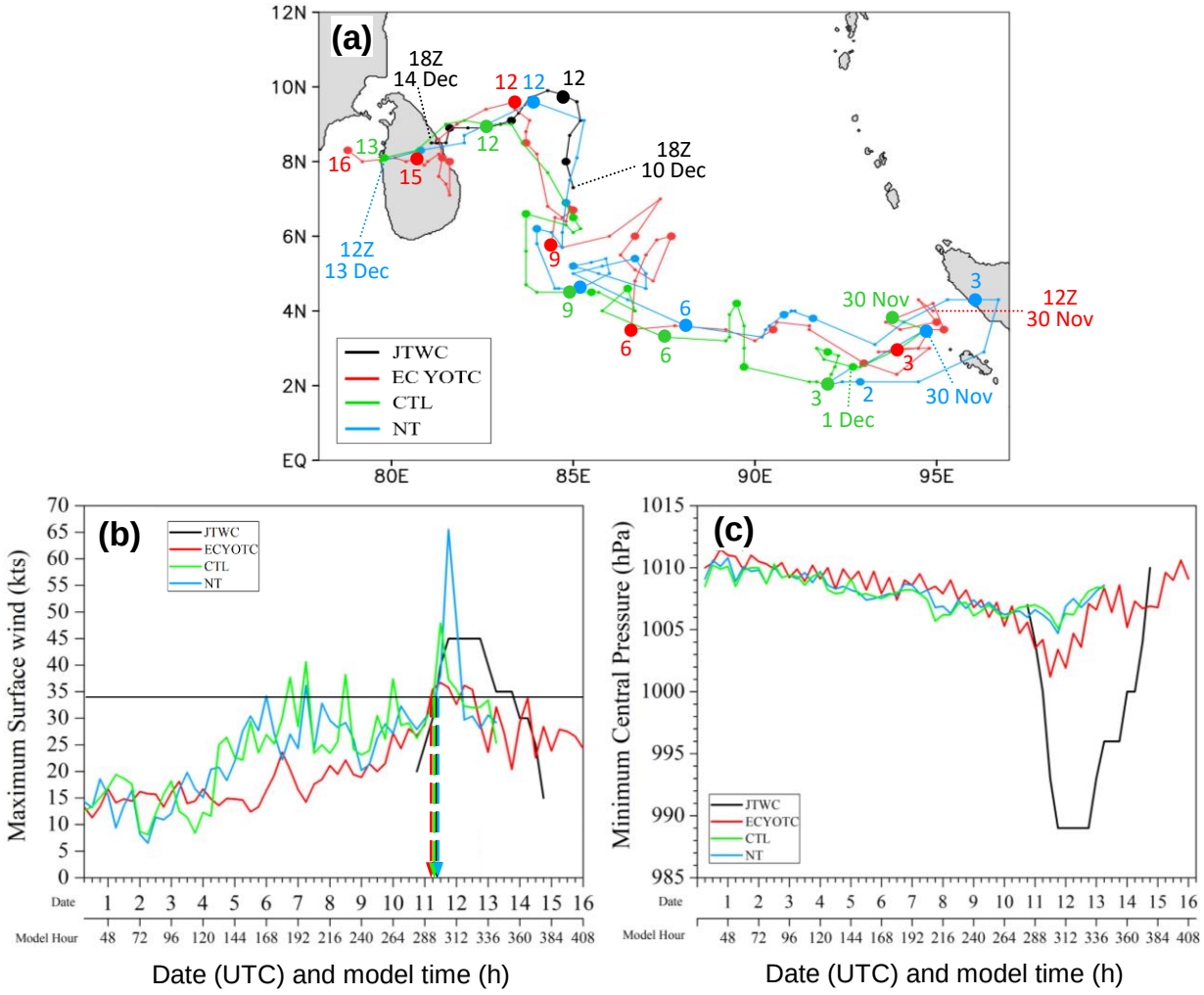

1 FIG. 11. As in Fig. 6, except for the case of TC Ward (30 Nov to 16 Dec 2009).

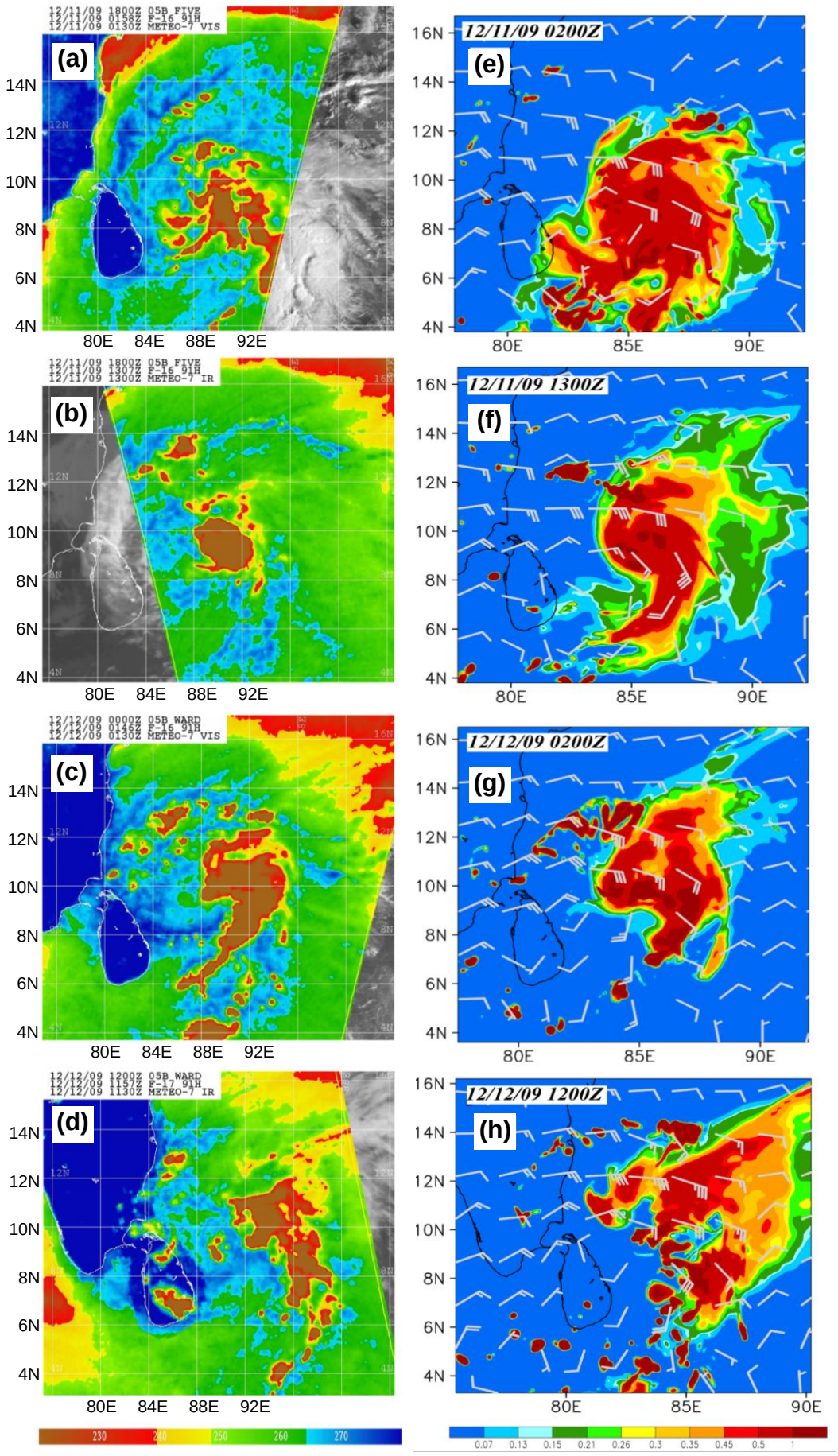
12/11/09 1800Z 05B FIVE
12/11/09 1158Z F-16 91H
12/11/09 1130Z METEO-7 VIS
(a)
12/11/09 1800Z 05B FIVE
12/11/09 1307Z F-16 91H
12/11/09 1300Z METEO-7 IR
(b)
12/12/09 0000Z 05B WARD
12/12/09 0146Z F-16 91H
12/12/09 0130Z METEO-7 VIS
(c)
12/12/09 1200Z 05B WARD
12/12/09 1157Z F-17 91H
12/12/09 1130Z METEO-7 IR
(d)
14N
12N
10N
8N
6N
4N
80E
84E
88E
92E
230
240
250
260
270
12/11/09 0200Z
(e)
12/11/09 1300Z
(f)
12/12/09 0200Z
(g)
12/12/09 1200Z
(h)
16N
14N
12N
10N
8N
6N
4N
80E
85E
90E
0.07
0.13
0.15
0.21
0.26
0.3
0.35
0.45
0.5
1

FIG. 12. As in Fig. 7, except for Ward at (a) 0158 and (b) 1307 UTC 11 Dec, and (c) 0146 and (d) 1157 UTC 12 Dec 2009 (source: NRL), and (e)-(h) from CTL at full hours closest to (a)-(d) as labeled, respectively.

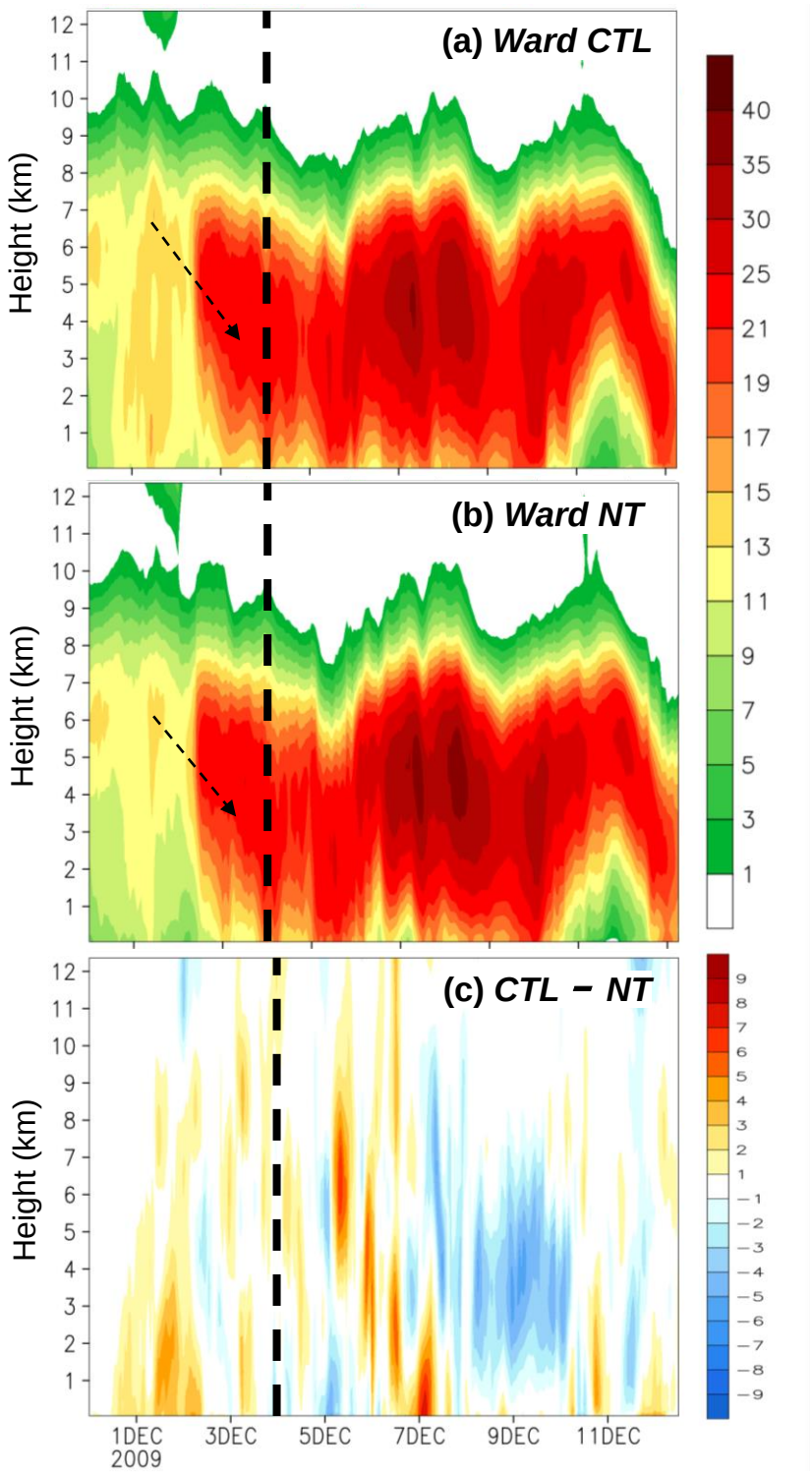

1 Fig. 13. As in Fig. 8, except for the case of TC Ward.

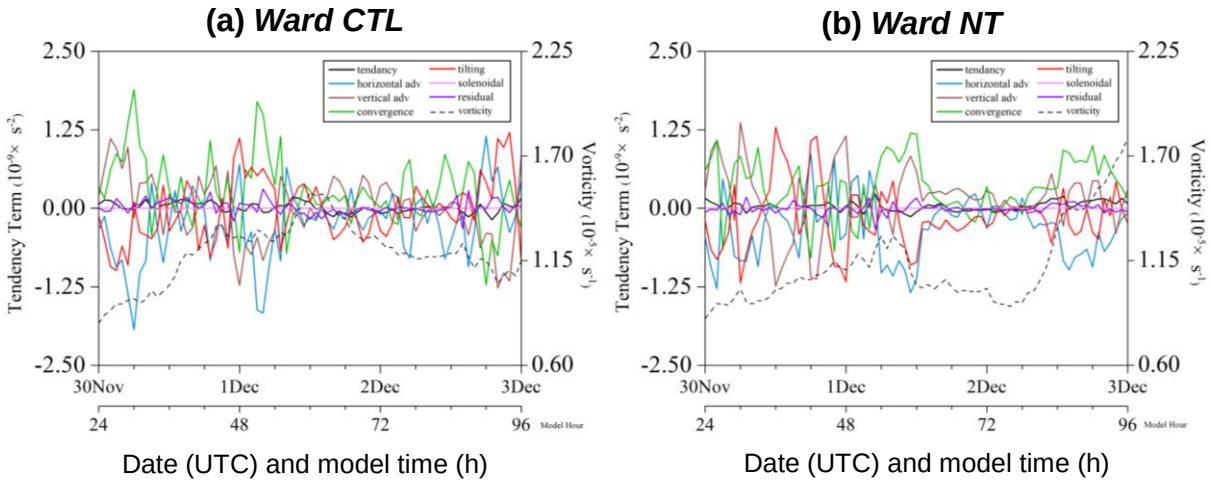

1 FIG. 14. As in Fig. 9, except for Ward from 0000 UTC 30 Nov to 0000 UTC 3 Dec 2009.

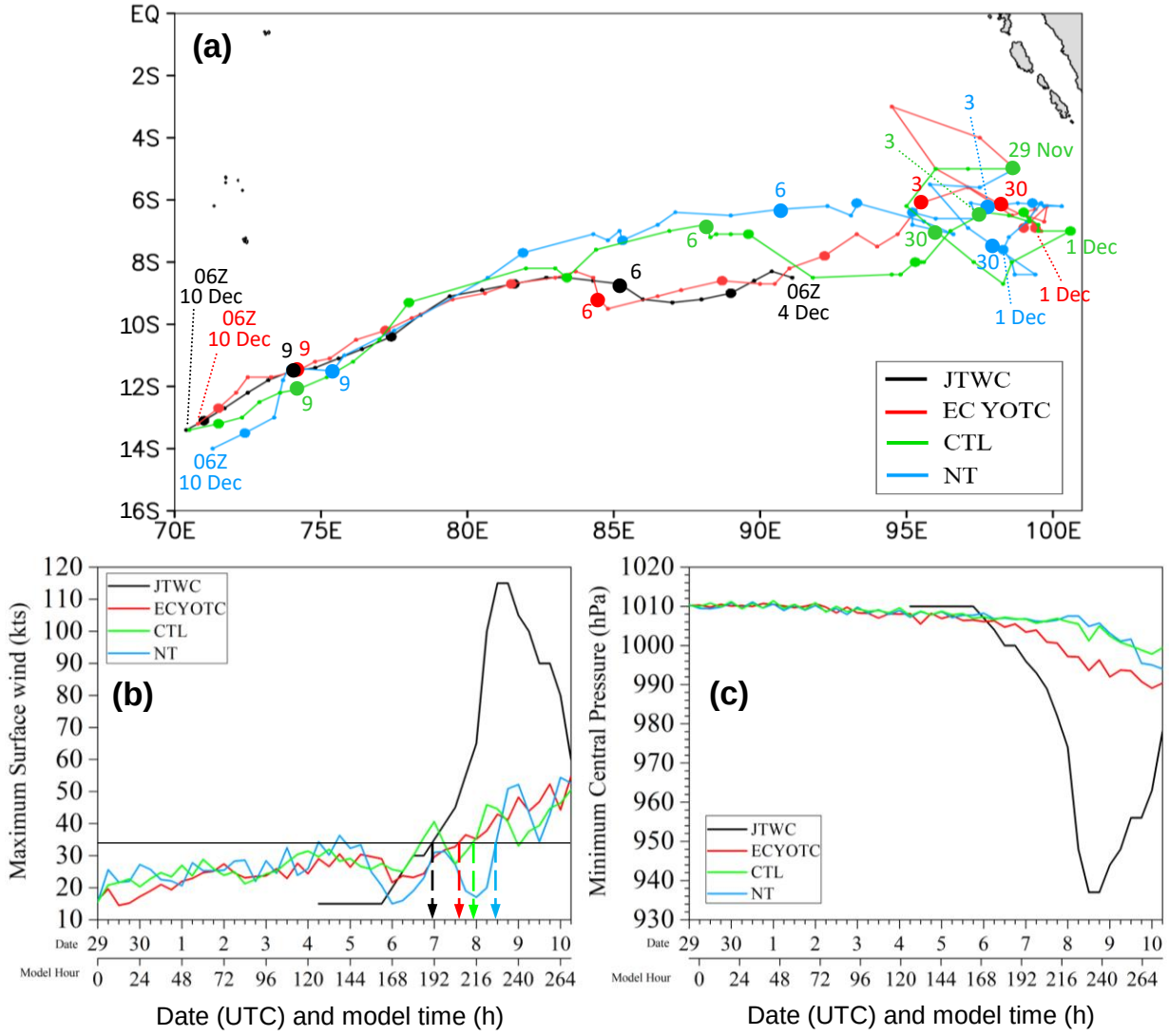

1 FIG. 15. As in Fig. 6, except for the case of TC Cleo (29 Nov to 10 Dec 2009).

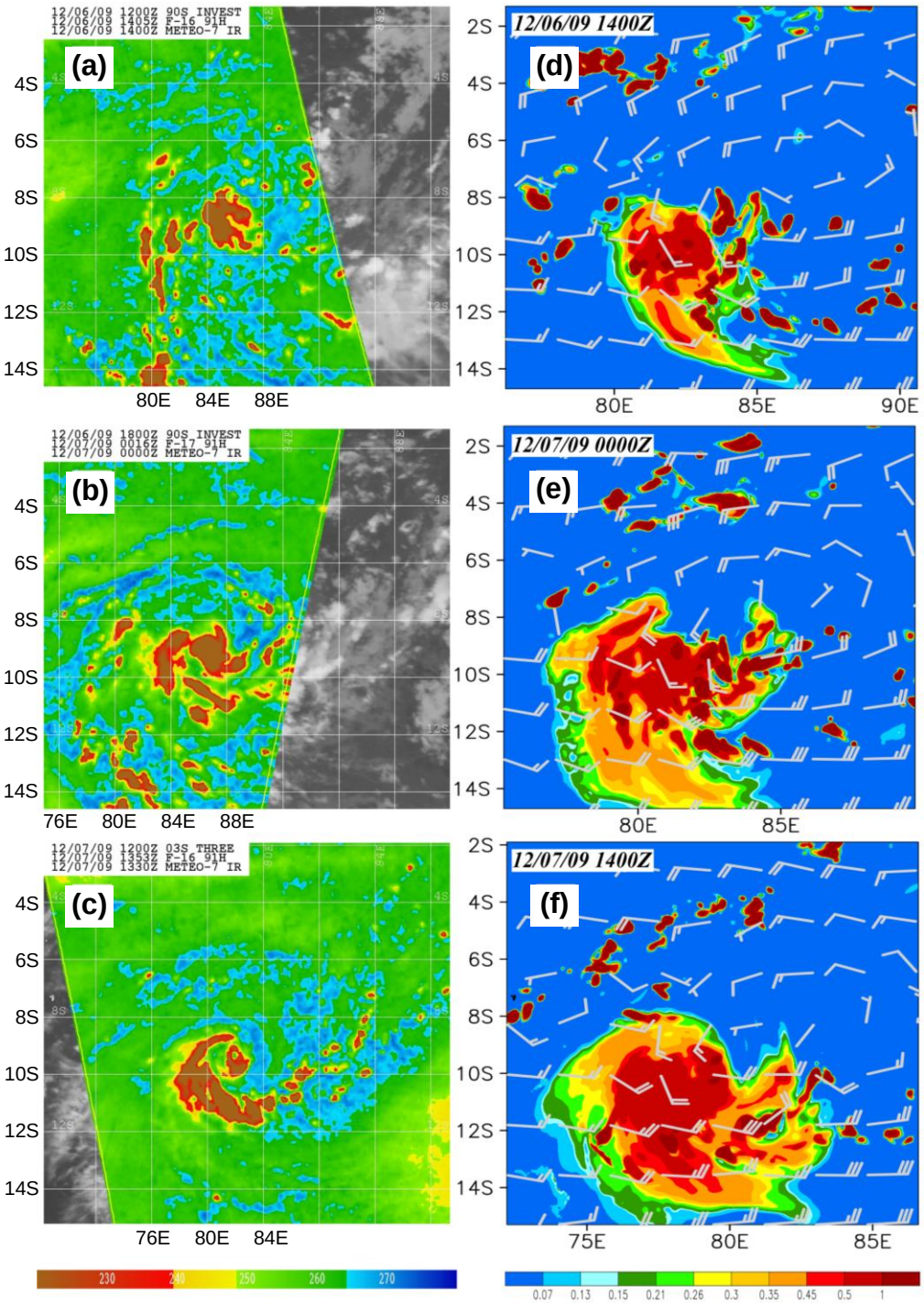

1 FIG. 16. As in Fig. 7, except for Cleo at (a) 1405 UTC 6 Dec, and (b) 0016 and (c) 1353 UTC
2 7 Dec 2009 (source: NRL), and (d)-(f) from CTL at full hours closest to (a)-(c) as labeled,
3 respectively.

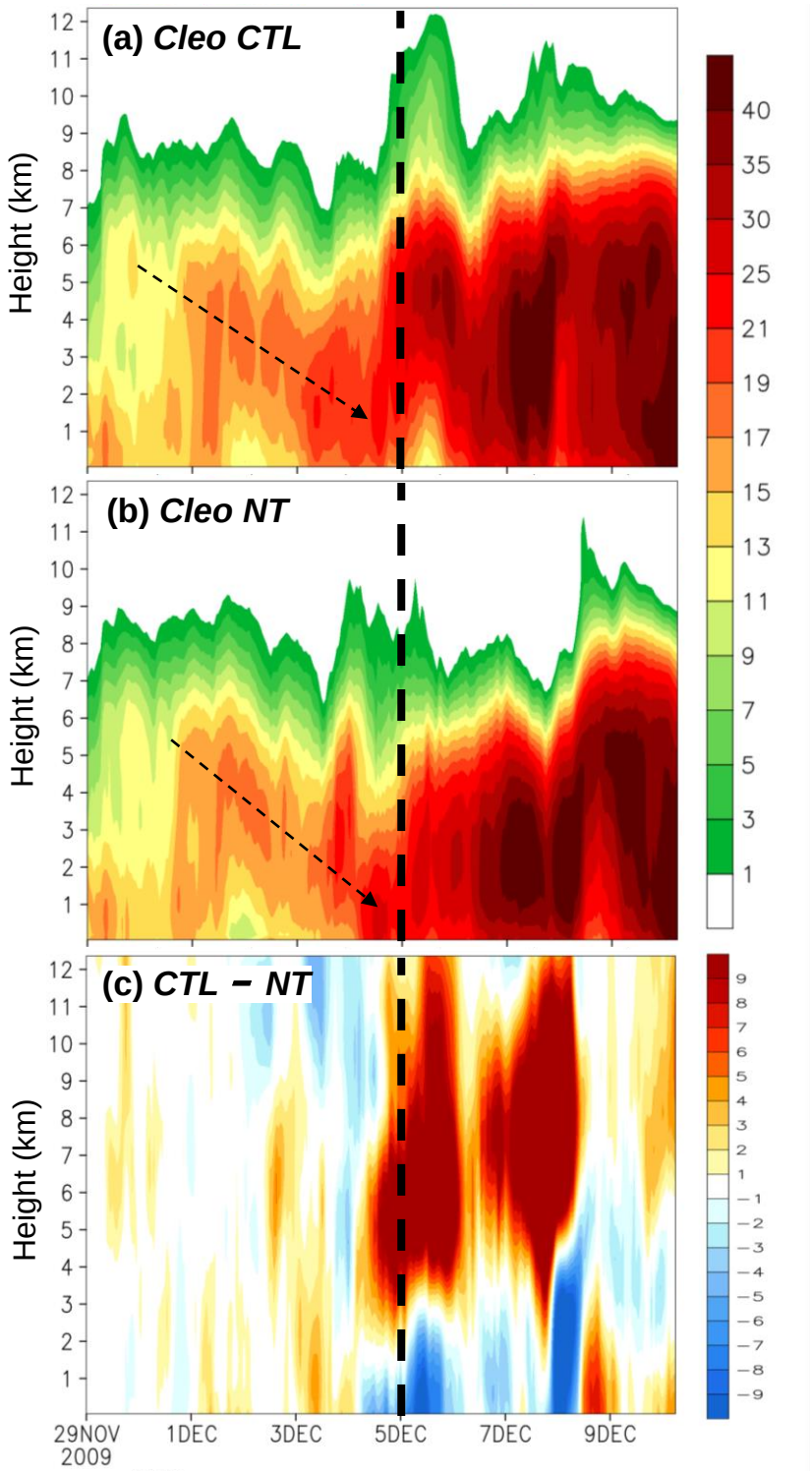

1 FIG. 17. As in Fig. 8, except for the case of TC Cleo.

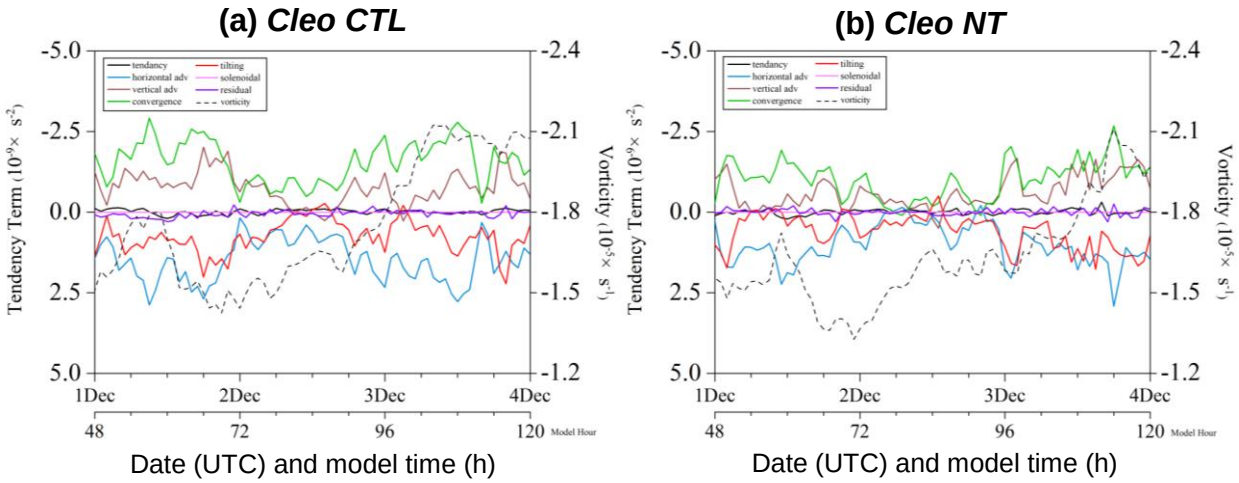

1 FIG. 18. As in Fig. 9, except for Cleo from 0000 UTC 1 Dec to 0000 UTC 4 Dec 2009. Note

2 that the vertical scale is reversed for this case in the Southern Hemisphere.

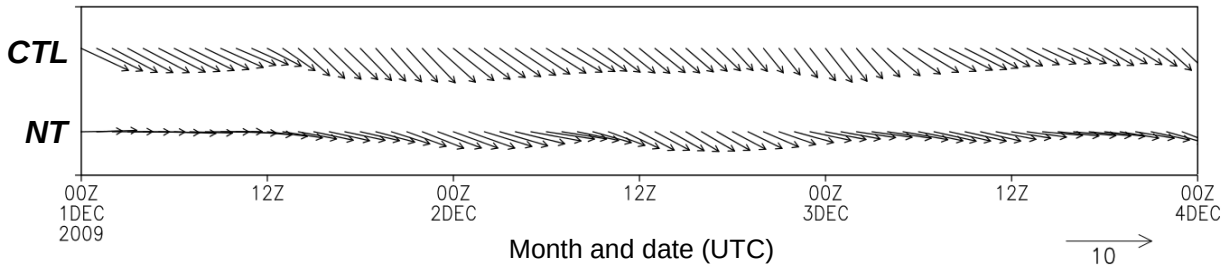

1 FIG. 19. Averaged low-level horizontal wind (m s^{-1}, over 50-1913 m) in the northeastern
2 quadrant of Cleo at 1-h intervals from 0000 UTC 1 Dec to 0000 UTC 4 Dec 2009 in
3 CTL and NT experiments.

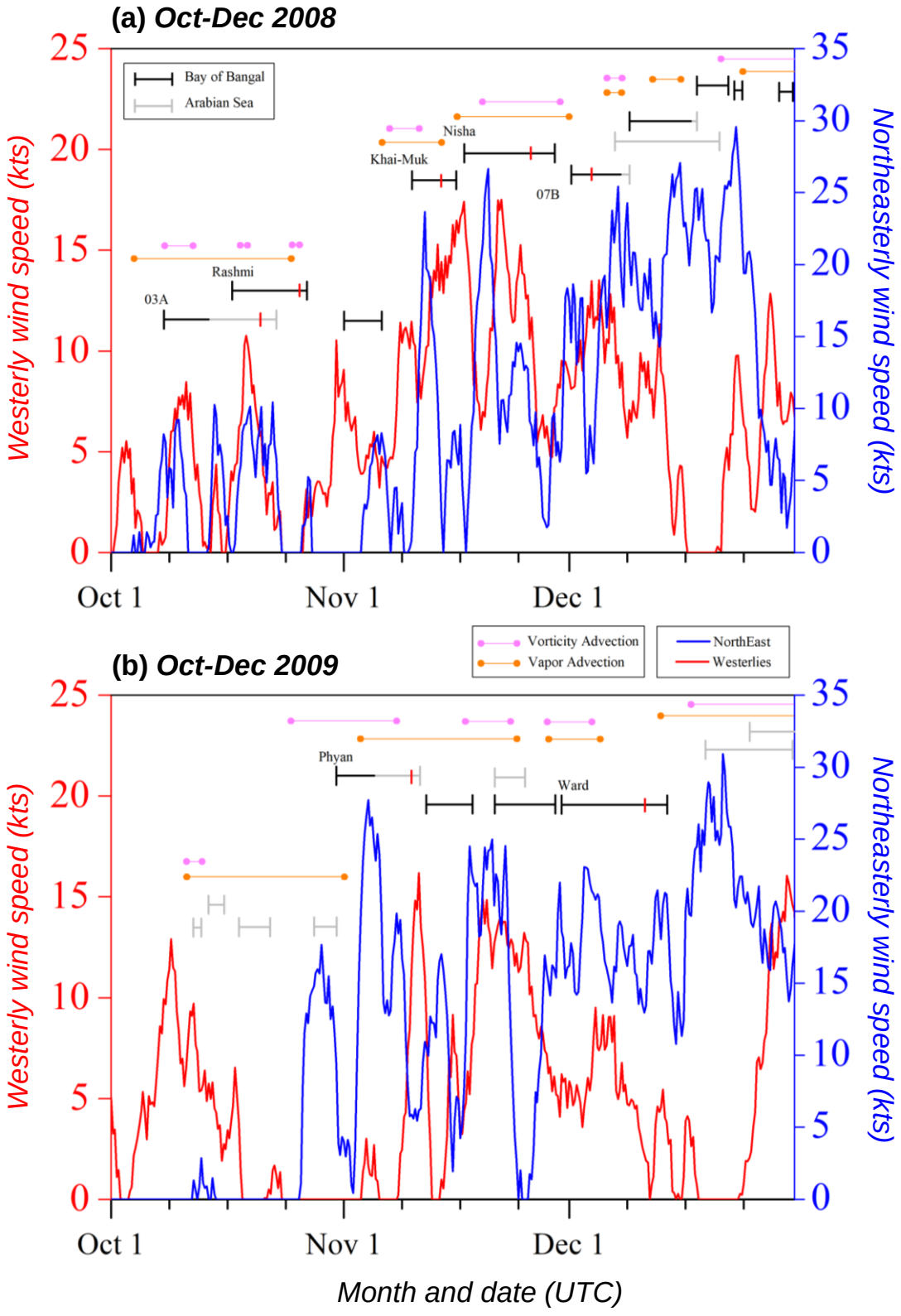

1 FIG. 20. Time-series of westerly wind speed in equatorial IO (kts, red, averaged over 5°S-5°N,
2 80°-90°E) and northeasterly wind speed east of northern Sumatra (kts, blue, averaged
3 over 5°-10°N, 107°-115°E) at 925 hPa in the ECMWF-YOTC data during Oct-Dec of (a)
4 2008 and (b) 2009. Black/gray segments indicate periods with closed vortex in BOB/AS

(divided at 80°E) with named storms labeled (the naming times shown by short red ticks). The periods with 700-hPa positive vorticity advection (pink) and moisture advection (orange) at the SCS are also marked.

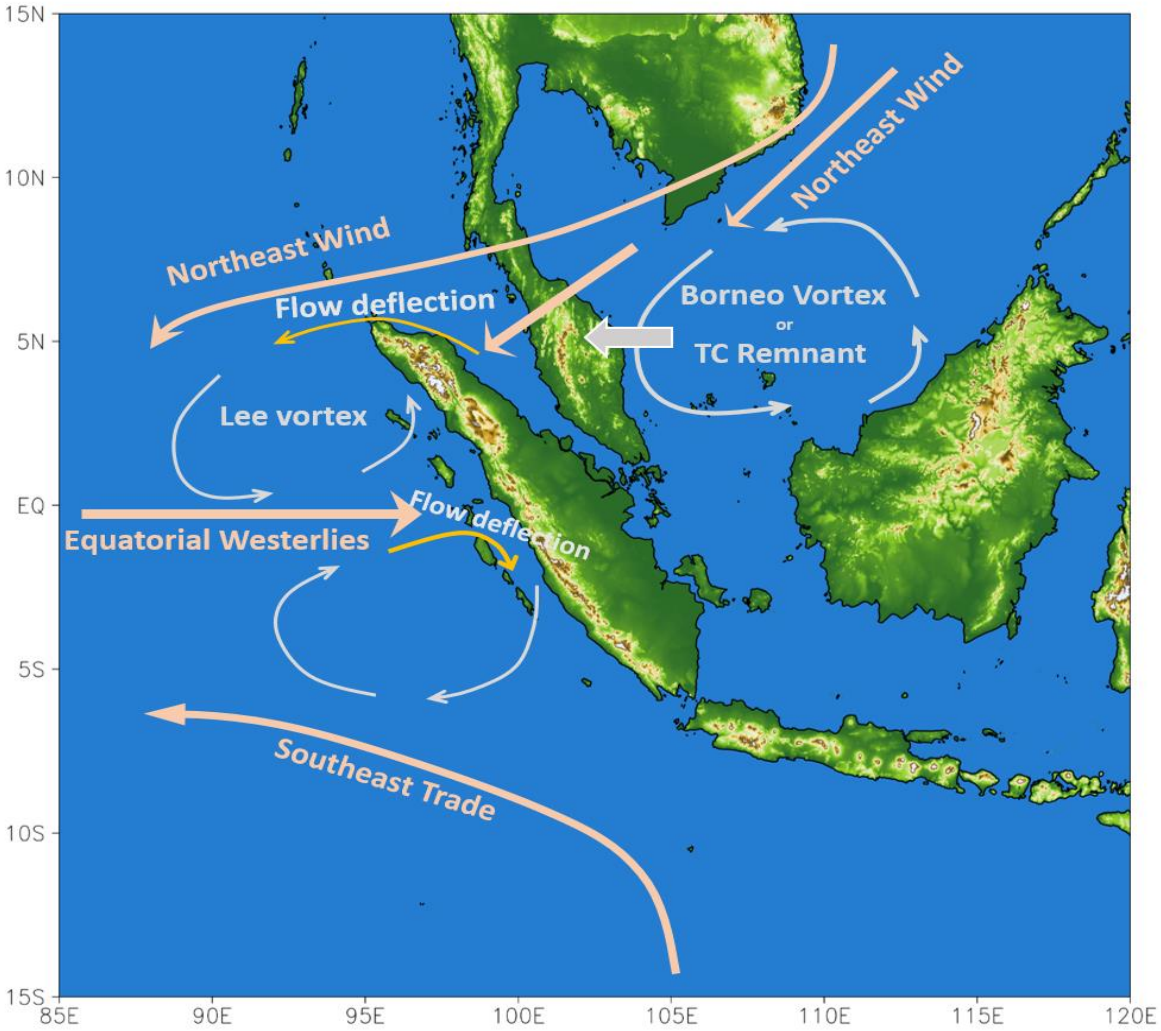

1 FIG. 21. Schematics for synoptic conditions favorable for the formation of lee vortices to the
2 west of Sumatra that may subsequently develop into TCs in the IO during the
3 post-monsoon period (Oct-Dec), obtained in this study. These factors include vorticity
4 and moisture advection from the SCS (linked to TC remnant or BV), prevailing
5 northeasterly (southeasterly) winds in NH (SH), and the deflection of low-level
6 northeasterly wind by the northern part (westerly wind by the southern part) of Sumatra
7 for the northern (southern) vortex.